CORONAVIRUS

Cannabidiol inhibits SARS-CoV-2 replication through induction of the host ER stress and innate immune responses

Long Chi Nguyen[1]†, Dongbo Yang[1]†, Vlad Nicolaescu[2,3]†, Thomas J. Best[4]†, Haley Gula[2,3], Divyasha Saxena[5], Jon D. Gabbard[5], Shao-Nong Chen[6], Takashi Ohtsuki[6]‡, John Brent Friesen[6], Nir Drayman[7], Adil Mohamed[7], Christopher Dann[1], Diane Silva[8], Lydia Robinson-Mailman[1], Andrea Valdespino[1], Letícia Stock[1], Eva Suárez[1], Krysten A. Jones[9], Saara-Anne Azizi[9], Jennifer K. Demarco[5], William E. Severson[5], Charles D. Anderson[5], James Michael Millis[10], Bryan C. Dickinson[9], Savaş Tay[7], Scott A. Oakes[8], Guido F. Pauli[6], Kenneth E. Palmer[5], The National COVID Cohort Collaborative Consortium§, David O. Meltzer[4], Glenn Randall[2,3]*, Marsha Rich Rosner[1]*

The spread of severe acute respiratory syndrome coronavirus 2 (SARS-CoV-2) and ongoing coronavirus disease 2019 (COVID-19) pandemic underscores the need for new treatments. Here, we report that cannabidiol (CBD) inhibits infection of SARS-CoV-2 in cells and mice. CBD and its metabolite 7-OH-CBD, but not THC or other congeneric cannabinoids tested, potently block SARS-CoV-2 replication in lung epithelial cells. CBD acts after viral entry, inhibiting viral gene expression and reversing many effects of SARS-CoV-2 on host gene transcription. CBD inhibits SARS-CoV-2 replication in part by up-regulating the host IRE1α ribonuclease endoplasmic reticulum (ER) stress response and interferon signaling pathways. In matched groups of human patients from the National COVID Cohort Collaborative, CBD (100 mg/ml oral solution per medical records) had a significant negative association with positive SARS-CoV-2 tests. This study highlights CBD as a potential preventative agent for early-stage SARS-CoV-2 infection and merits future clinical trials. We caution against current use of non-medical formulations as a preventative or treatment therapy.

INTRODUCTION

Severe acute respiratory syndrome coronavirus 2 (SARS-CoV-2) is responsible for coronavirus disease 2019 (COVID-19), a pandemic that continues to cause widespread morbidity and mortality across the globe. SARS-CoV-2 is the seventh species of coronavirus known to infect people. These coronaviruses, which include SARS-CoV, 229E, NL63, OC43, HKU1, and Middle East respiratory syndrome coronavirus (MERS-CoV), cause a range of symptoms from the common cold to more severe pathologies (*1*). Despite recent vaccine availability, SARS-CoV-2 is still spreading rapidly (*2*), highlighting the need for alternative treatments, especially for populations with limited inclination or access to vaccines. To date, few therapies have been identified that block SARS-CoV-2 replication and viral production.

SARS-CoV-2 is a positive-sense single-stranded RNA enveloped virus composed of a lipid bilayer and four structural proteins that drive viral particle formation. The spike (S), membrane (M), and envelope (E) are integral proteins of the virus membrane and promote virion budding while also recruiting the nucleocapsid (N) protein and the viral genomic RNA into nascent virions. Like its close relative SARS-CoV, SARS-CoV-2 primarily enters human cells by the binding of the viral S protein to the angiotensin converting enzyme 2 (ACE2) receptor (*3*–*5*), after which the S protein undergoes proteolysis by transmembrane protease serine 2 (TMPRSS2) or other proteases into two noncovalently bound peptides (S1 and S2) that facilitate viral entry into the host cell. The N-terminal S1 binds the ACE2 receptor, and the C-terminal S2 mediates viral–cell membrane fusion following proteolytic cleavage. Depending on the cell type, viral entry can also occur after ACE2 binding, independent of proteolytic cleavage (*6*–*8*). Following cell entry, the SARS-CoV-2 genome is translated into two large polypeptides that are cleaved by two viral proteases, Mpro and PLpro (*9*, *10*), to produce 15 proteins, in addition to the synthesis of subgenomic RNAs that encode another 10 accessory proteins plus the 4 structural proteins. These proteins enable viral replication, assembly, and budding. In an effort to suppress infection by the SARS-CoV-2 β-coronavirus as well as other evolving pathogenic viruses, we tested the antiviral potential of a number of small molecules that target host stress response pathways.

One potential regulator of the host stress and antiviral inflammatory responses is cannabidiol (CBD), a member of the cannabinoid class of natural products (*11*) produced by *Cannabis sativa* (Cannabaceae; marijuana/hemp). Hemp refers to cannabis plants

[1]Ben May Department for Cancer Research, University of Chicago, Chicago, IL 60637, USA. [2]Department of Microbiology, University of Chicago, Chicago, IL 60637, USA. [3]Howard Taylor Ricketts Laboratory, Argonne National Laboratory, Lemont, IL 60439, USA. [4]Center for Health and the Social Sciences, University of Chicago, Chicago, IL 60637, USA. [5]Center for Predictive Medicine for Biodefense and Emerging Infectious Diseases, University of Louisville, Louisville, KY 40222, USA. [6]Pharmacognosy Institute and Department of Pharmaceutical Sciences, College of Pharmacy, University of Illinois at Chicago, Chicago, IL 60612, USA. [7]Pritzker School of Molecular Engineering, University of Chicago, Chicago, IL 60637, USA. [8]Department of Pathology, University of Chicago, Chicago, IL 60637, USA. [9]Department of Chemistry, University of Chicago, Chicago, IL 60637, USA. [10]Department of Surgery, University of Chicago, Chicago, IL 60637, USA.
*Corresponding author. Email: grandall@bsd.uchicago.edu (G.R.); mrosner@uchicago.edu (M.R.R.)
†These authors contributed equally to this work.
‡Present address: Department of Food Bioscience and Biotechnology, College of Bioresource Sciences, Nihon University, Fujisawa, Kanagawa, Japan.
§Consortium authors and affiliations are provided in the Supplementary Materials.

or materials derived thereof that contain 0.3% or less of the psychotropic tetrahydrocannabinol (THC) and typically have relatively high CBD content. By contrast, marijuana refers to *C. sativa* materials with more than 0.3% THC by dry weight. THC acts through binding to the cannabinoid receptor, and CBD potentiates this interaction (*11*). Despite numerous studies and many unsubstantiated claims related to CBD-containing products, the biologic actions of CBD itself are unclear and specific targets are mostly unknown (*12*). However, an oral solution of CBD is a U.S. Food and Drug Administration (FDA)–approved drug, largely for the treatment of epilepsy (*13*). Thus, CBD has drug status, is viable as a therapeutic, and cannot be marketed as a dietary supplement in the United States (*12*). Although limited, some studies have reported that certain cannabinoids have antiviral effects against hepatitis C virus and other viruses (*14*).

RESULTS

High-purity CBD inhibits SARS-CoV-2 replication in human lung epithelial cells

To test the effect of CBD on SARS-CoV-2 replication, we pretreated A549 human lung carcinoma cells expressing exogenous human ACE2 receptor (A549-ACE2) for 2 hours with 0 to 10 μM CBD before infection with SARS-CoV-2. After 48 hours, we monitored cells for expression of the viral spike protein (S) and viral titer. CBD potently inhibited viral replication under nontoxic conditions with a median effective concentration (EC_{50}) of ~1 μM (Fig. 1A and fig. S1A). CBD inhibited SARS-CoV-2 replication in human Calu3 lung and Vero E6 monkey kidney epithelial cells as well (fig. S1B), and no toxicity was observed at the effective doses (fig. S1, C and D). Last, we tested three SARS-CoV-2 variants of concern (α, β, and γ) in addition to the original SARS-CoV-2 strain, and their ability to infect cells was comparably inhibited by CBD (Fig. 1C).

When isolated from its source plant, natural nonsynthetic CBD is typically extracted along with other cannabinoids, representing the unavoidable residual complexity of natural products (*12*). To verify that CBD is indeed responsible for the viral inhibition, we analyzed a CBD reference standard as well as CBD from four different sources for purity using 100% quantitative nuclear magnetic resonance (qNMR). These sources included two chemical vendors (suppliers A and B) and two commercial vendors (suppliers C and D). The notable congruence between the experimental ^{1}H NMR and the recently established quantum-mechanical HiFSA (^{1}H Iterative Full Spin Analysis) profiles observed for all materials confirmed that (i) the compounds used were indeed CBD with purities of at least 97% (Fig. 1B) and (ii) congeneric cannabinoids were not present at levels above 1.0%. Analysis of these different CBD samples in the viral A549-ACE2 infection assay showed similar EC_{50}s with a range from 0.6 to 1.8 μM, likely reflecting the intrinsic variability of the biological assay (Fig. 1A). No toxicity was observed for any of the CBD preparations at the doses used to inhibit viral infection (fig. S1, E to G).

The CBD metabolite 7-OH-CBD, but not a panel of closely related CBD congeners, exhibits antiviral activity

CBD is often consumed as part of a *C. sativa* extract, particularly in combination with psychoactive THC enriched in marijuana plants. We therefore determined whether congeneric cannabinoids, especially analogs with closely related structures and polarities produced by the hemp plant, are also capable of inhibiting SARS-CoV-2

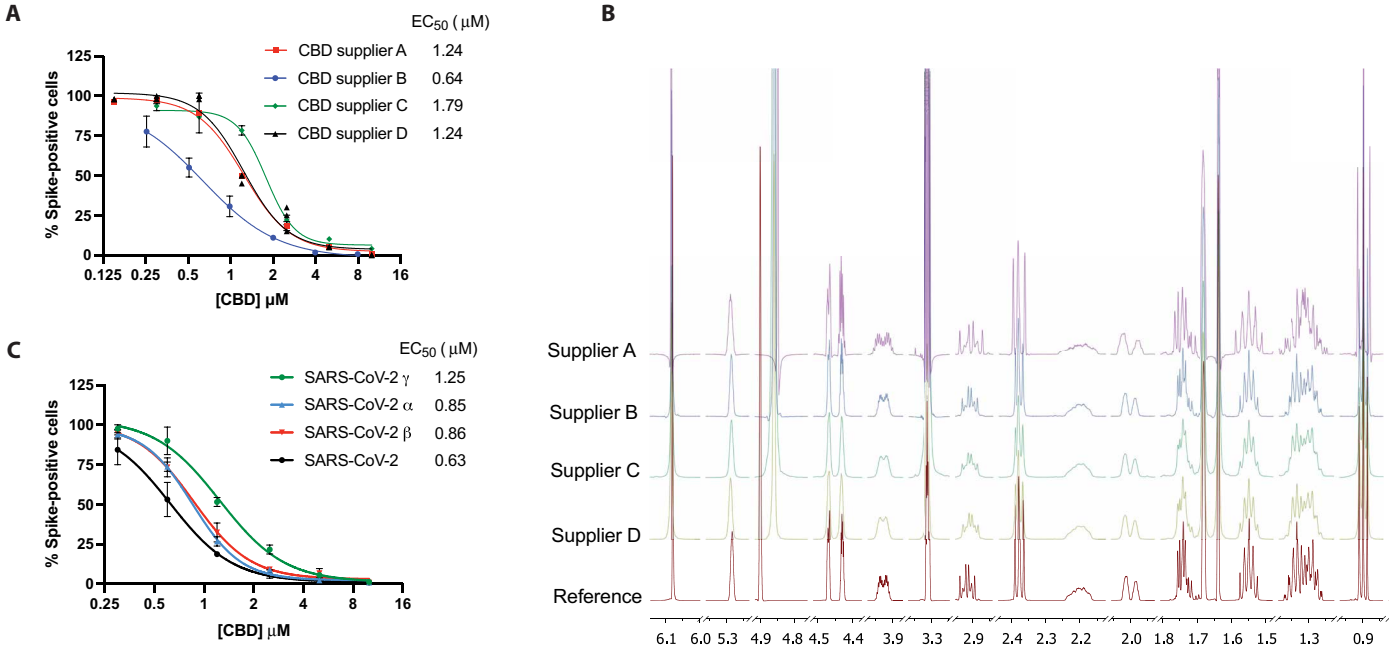

Fig. 1. CBD is a potent inhibitor of SARS-CoV-2 infection in vitro. (**A**) A549-ACE2 cells were treated with indicated doses of CBD from four different suppliers, followed by infection with SARS-CoV-2 at an MOI of 0.5 for 48 hours. The cells were stained for spike protein, and the percentage of cells expressing the spike protein in each condition was plotted. EC_{50} values are indicated. (**B**) The ^{1}H qNMR spectra of CBD reference material and CBD samples from four different suppliers. (**C**) A549-ACE2 cells were treated with CBD from supplier A, followed by infection with SARS-CoV-2 or α, β, or γ variants at an MOI of 0.5 for 48 hours. The cells were stained for spike protein, and the percentage of cells expressing the spike protein in each condition was plotted. EC_{50} values are indicated.

infection. Of this group, only CBD was a potent agent, while no or very limited antiviral activity was exhibited by these structurally closely related congeners that share biosynthesis pathways and form the biogenetically determined residual complexity of CBD purified from *C. sativa*: THC, cannabidiolic acid (CBDA), cannabidivarin (CBDV), cannabichromene (CBC), or cannabigerol (CBG) (Fig. 2, A and D; see Materials and Methods). None of these cannabinoids were toxic to the A549-ACE2 cells in the dose range of interest (fig. S2). Notably, combining CBD with THC (1:1) significantly suppressed CBD efficacy, consistent with competitive inhibition by THC.

CBD is rapidly metabolized in the intestine and liver into two main metabolites, 7-carboxy-cannabidiol (7-COOH-CBD) and 7-hydroxy-cannabidiol (7-OH-CBD). The level of 7-COOH-CBD is 40-fold higher, and the level of 7-OH-CBD is 38% of the CBD level in human plasma (*15*). CBD and its 7-OH-CBD metabolite are the active and equipotent ingredients for the treatment of epilepsy (*13*). Like CBD, 7-OH-CBD effectively inhibited SARS-CoV-2 replication in A549-ACE2 cells (Fig. 2C) and was nontoxic to cells (fig. S2, H and I). Analysis of blood plasma levels in healthy individuals taking 1500 mg daily of FDA-approved CBD solution (Epidiolex) showed a maximal concentration (C_{max}) at 7 days for CBD and 7-OH-CBD of 1.7 and 0.56 μM, respectively; the C_{max} can be further increased several-fold by coadministration with a high-fat meal (*15*). Taken in aggregate, these results suggest that the effective plasma concentrations of CBD and its metabolite are within the therapeutic range to inhibit SARS-CoV-2 infection in humans.

CBD acts at an early step after viral entry into cells

CBD could be acting by blocking viral entry to host cells or at later steps following infection. As CBD was reported to decrease ACE2 expression in some epithelial cells, including A549 (*16*), we first determined whether CBD suppressed the SARS-CoV-2 receptor in the A549-ACE2, Calu-3, and Vero E6 cells. No decrease in ACE2 expression was observed (Fig. 3A and fig. S4, A and B). Furthermore, analysis of lentiviruses pseudotyped with either the SARS-CoV-2 spike protein or the vesicular stomatitis virus (VSV) glycoprotein (*17*) showed that 10 μM CBD only weakly inhibited cell entry by spike-expressing virus, suggesting that other mechanisms are largely responsible for its antiviral effects. The robustness of the assay was confirmed by using anti-spike antibodies that effectively blocked viral infection of lentivirus pseudotyped with spike, but not VSVg (Fig. 3B and fig. S3, A and B). In contrast to the negligible effect on viral entry, CBD was very effective (~95 to 99%) at inhibiting SARS-CoV-2 spike protein expression in host cells at 2 and 6 hours after infection after entry (Fig. 3C). This was true even in the presence of antibodies to the spike protein to prevent reinfection (Fig. 3D),

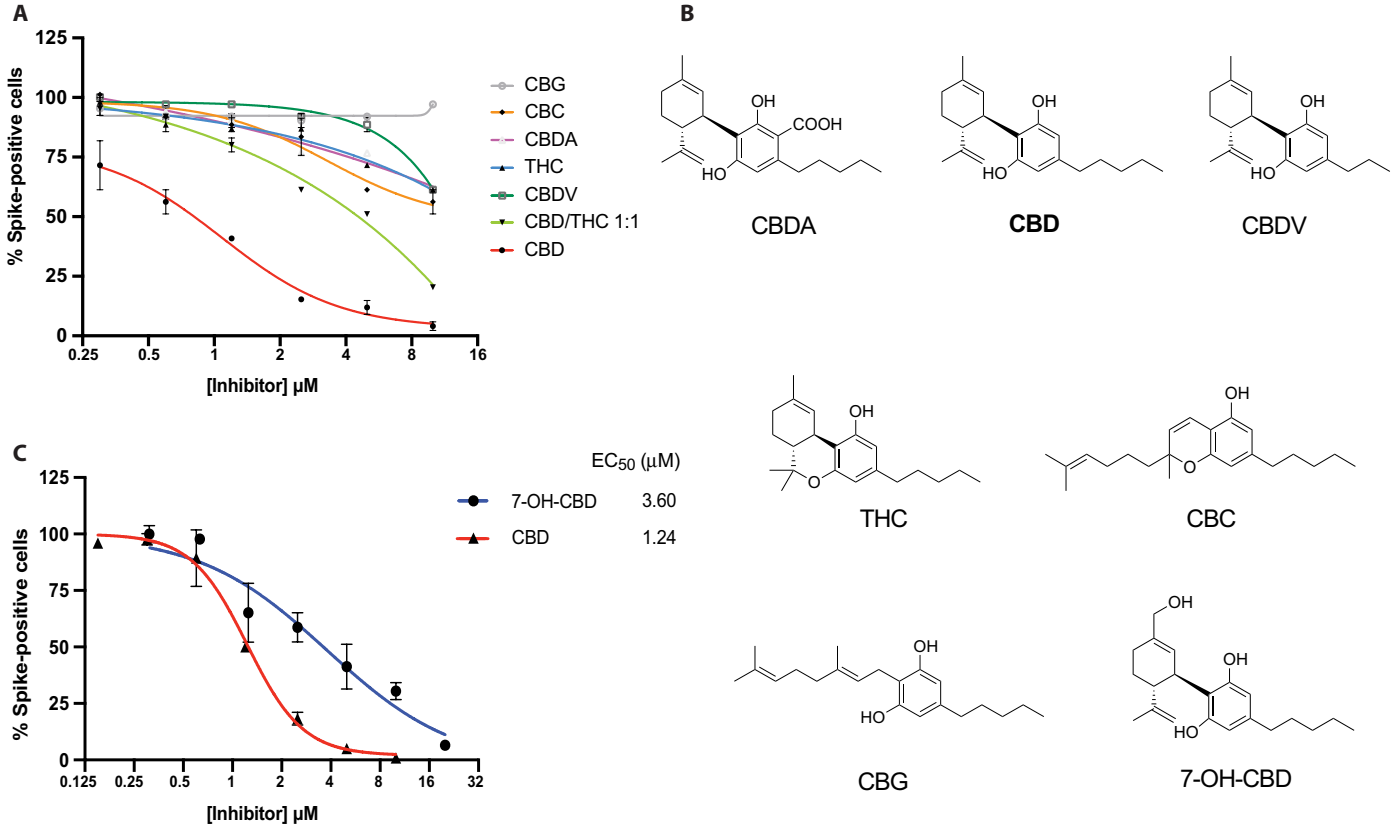

Fig. 2. Limited or no inhibition of SARS-CoV-2 infection by cannabinoids other than CBD. (**A**) A549-ACE2 cells were treated with indicated doses of various cannabinoids or a CBD/THC 1:1 mixture, followed by infection with SARS-CoV-2 at an MOI of 0.5 for 48 hours. The cells were stained for spike protein, and the percentage of cells expressing the spike protein in each condition was plotted. All cannabinoids tested were isolated from a hemp extract as described in Materials and Methods. (**B**) Chemical structures of cannabinoids and 7-OH-CBD. (**C**) A549-ACE2 cells were treated with indicated doses of 7-OH-CBD, followed by infection with the SARS-CoV-2 at an MOI of 0.5. The cells were stained for spike protein, and the percentage of cells expressing the spike protein in each condition was plotted. Representative data of CBD from Fig. 1C (supplier A) are used for comparison. EC_{50} values are indicated.

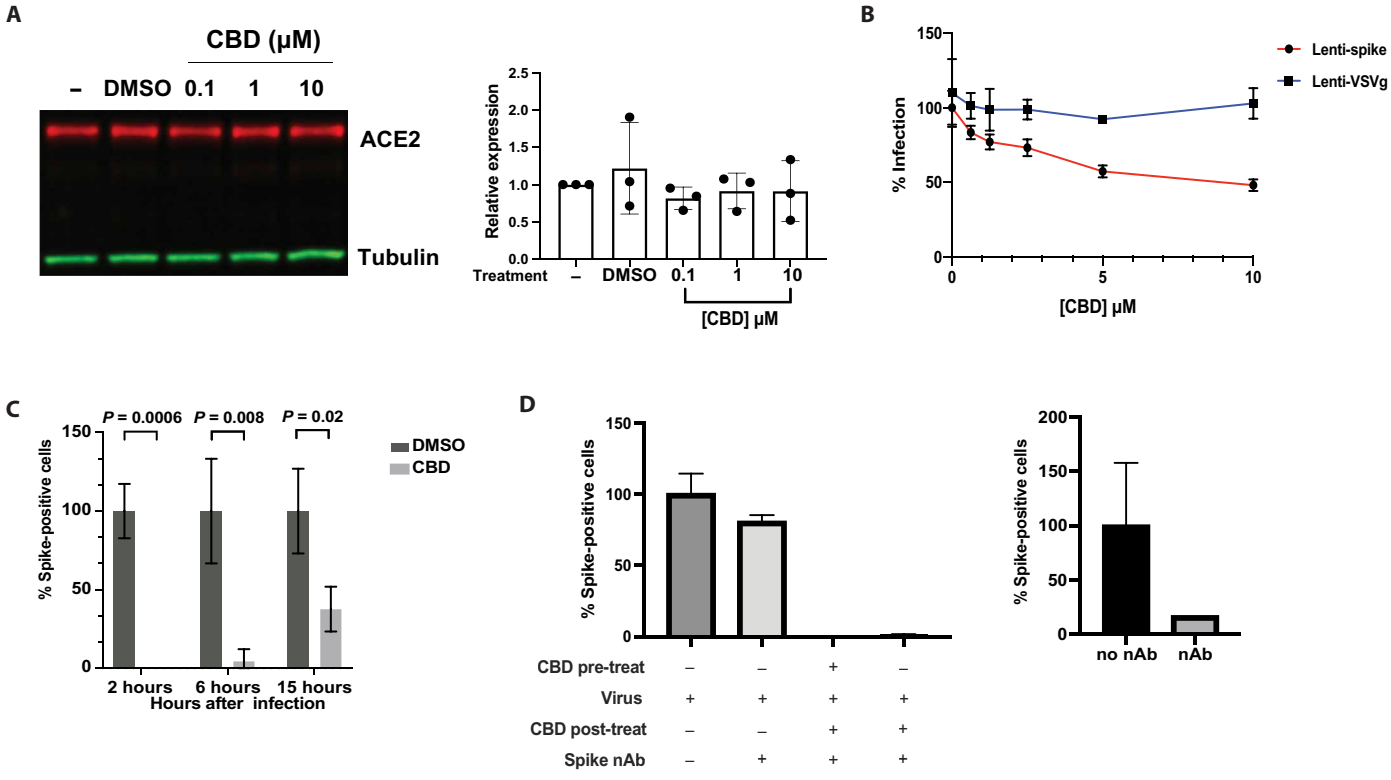

Fig. 3. CBD inhibits viral replication after SARS-CoV-2 entry into the host cell. (**A**) Immunoblots of ACE2 protein expression from A549-ACE2 cell lysates either untreated or treated with vehicle or CBD at indicated doses ($n = 3$). Blots were probed with antibodies against ACE2 and tubulin. ACE2 protein expression levels were normalized to the tubulin signal within each sample. ACE2 expression levels were plotted relative to untreated samples. DMSO, dimethyl sulfoxide. (**B**) 293 T–ACE2 cells were infected by spike or VSV-G pseudovirus for 72 hours with the indicated doses of CBD treatment, and the percentages of infected cells were plotted. (**C**) A549-ACE2 cells were infected with SARS-CoV-2 at an MOI of 0.5 for 2 hours. DMSO or 10 μM CBD was then added at either 2, 6, or 15 hours after infection. After 16 hours, spike-positive cells were quantified and normalized to the virus-infected only samples. (**D**) Left: A549-ACE2 cells were infected with SARS-CoV-2 at an MOI of 0.5 for 2 hours. DMSO or 10 μM CBD was then added at 2 hours after infection with the spike neutralizing antibody (nAb) to prevent reinfection. After 16 hours, spike-positive cells were quantified and normalized to the virus-infected only samples. Right: Validation of neutralizing antibody efficacy. SARS-CoV-2 virus (400 PFU) was incubated with or without 100 nM neutralizing antibody for 1 hour. A549-ACE2 cells were treated with the mixture for 16 hours, and spike-positive cells were quantified.

suggesting that CBD acts early in the infection cycle, in a postentry step. CBD was also partially effective (~60%) at inhibiting SARS-CoV-2 at 15 hours after infection (Fig. 3C), suggesting a possible secondary effect on viral assembly and release. To assess whether CBD might be preventing viral protein processing by the viral proteases Mpro or PLpro, we assayed their activity in vitro (fig. S4, C and D). CBD did not affect the activity of either protease, raising the possibility that CBD targets host cell processes.

CBD inhibits viral RNA expression and reverses viral-induced changes in host gene expression

Consistent with this interpretation, RNA sequencing (RNA-seq) analysis of infected A549-ACE2 cells treated with CBD for 24 hours shows a notable suppression of SARS-CoV-2–induced changes in gene expression. CBD effectively eradicated viral RNA expression in the host cells, including RNA coding for spike, membrane, envelope, and nucleocapsid proteins (Fig. 4, A and B). Both SARS-CoV-2 and CBD each induced significant changes in cellular gene expression (figs. S5 and S6). Principal components analysis (PCA) of host cell RNA shows almost complete reversal of viral changes, but rather than returning to a normal cell state, the CBD + virus-infected cells resemble those treated with CBD alone (Fig. 4C). Clustering analysis using Metascape reveals some interesting patterns and associated themes (Fig. 4D and figs. S7 and S8). For example, viral induction of genes associated with chromatin modification and transcription (cluster 1) is reversed by CBD, although CBD alone has no effect. Similarly, viral inhibition of genes associated with ribosomes and neutrophils (cluster 3) is largely reversed by CBD, but the drug alone has no effect. This contrasts with clusters 5 and 6 where CBD alone induces strong activation of genes associated with the host stress response. Together, these results suggest that CBD acts to prevent viral protein translation and associated cellular changes.

To gain a better understanding of the specific antiviral action of CBD, we analyzed RNA-seq from lysates of uninfected or SARS-CoV-2–infected cells treated for 24 hours with the inactive CBDV homolog. Induction of viral genes for spike, envelope, and nucleocapsid proteins is reduced by only 60% with CBDV as opposed to ~99% with CBD (Fig. 5, A and B). CBDV treatment causes fewer transcriptomic changes than CBD in A549-ACE2 cells and is largely ineffective at reversing transcriptional changes induced by SARS-CoV-2 (Fig. 5C). Clustering analysis using Metascape reveals only a couple clusters that show CBDV reversal of viral transcriptomic changes (Fig. 5D). These include autophagy and lipid metabolism (cluster 1)

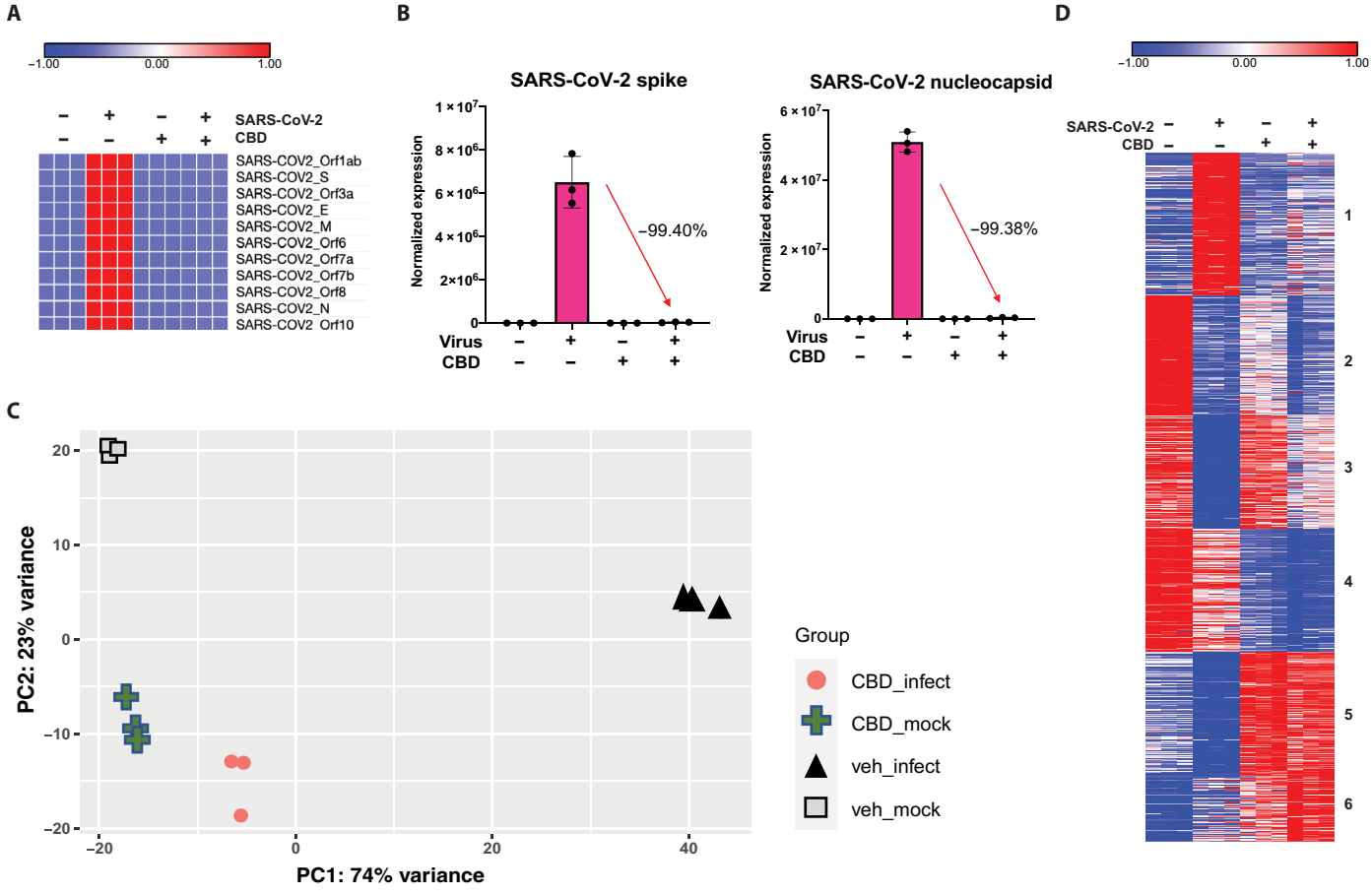

Fig. 4. Changes in viral and host cell transcription following SARS-CoV-2 infection or CBD treatment. A549-ACE2 cells were infected with SARS-CoV-2 at an MOI of 3 with or without CBD treatment at 10 μM for 24 hours. RNA-seq was performed as described in Materials and Methods. (**A**) Heatmap of relative levels of SARS-CoV-2 genes from the RNA-seq samples. (**B**) Expression levels of SARS-CoV-2 spike and nucleocapsid genes. Percent expression level changes for genes from infected cells compared to cells infected and CBD treated are indicated for each gene. (**C**) PCA of RNA-seq data showing control (veh_mock), SARS-CoV-2–infected (veh_infect), CBD-treated (CBD_mock), and SARS-CoV-2–infected plus CBD-treated (CBD_infect) samples. The first and second principal components (PC1 and PC2) of each sample are plotted. (**D**) Heatmap of normalized expression levels of 5000 most variable genes across all RNA-seq samples, clustered into six groups based on differential expression between treatment conditions.

that are induced by CBDV as well as protein translation/cell cycle/DNA replication (cluster 3) that are suppressed by CBDV.

CBD induces the ER stress response and IRE1α activity as a key mechanism for its antiviral action

Of particular interest are three sets of genes related to the endoplasmic reticulum (ER) stress response, the unfolded protein response (UPR), and interferon induction that are selectively upregulated by CBD but not CBDV (Fig. 6A). By contrast, genes associated with the oxidative stress response are induced by both cannabinoids. Cells experience ER stress when the workload on the ER protein folding machinery exceeds its capability. Under ER stress, secretory proteins accumulate in unfolded forms within the organelle to trigger a set of intracellular signaling pathways called UPR, which is part of a larger cellular stress response that maintains proteostasis throughout the cell (*18*). The UPR pathway is controlled by three ER transmembrane proteins—inositol-requiring enzyme-1α (IRE1α), protein kinase R-like endoplasmic reticulum kinase (PERK), and activating transcription factor 6 (ATF6)—that contain an ER luminal domain capable of directly or indirectly sensing misfolded proteins. In response to ER stress, each of these sensors sets in motion transcriptional and translational changes that increase protein folding capacity and attempt to restore homeostasis. However, if the stress on the ER is irremediable, then the UPR switches outputs and signals cell death. We validated CBD induction of IRE1α, PERK, and ATF6 gene expression by quantitative reverse transcription polymerase chain reaction (qRT-PCR) (fig. S9A), consistent with previous reports (*19*). Ingenuity analysis confirmed that CBD induces the UPR significantly more than CBDV (figs. S9B, S10B, and S11).

Numerous studies report compelling evidence that the UPR is hyperactivated and required for replication of other closely related coronavirus family members (*20*, *21*). Unexpectedly, although gene set enrichment analysis (GSEA) of the RNA-seq data showed that the IRE1α pathway is strongly activated by CBD in the presence or absence of virus, this pathway was not activated by SARS-CoV-2 alone (Table 1 and figs. S12 to S14). PERK, by contrast, was functionally activated by both SARS-CoV-2 and CBD. IRE1α is a single-pass ER transmembrane protein with bifunctional kinase/endoribonuclease [ribonuclease (RNase)] activities. In response to ER stress, IRE1α undergoes oligomerization and autophosphorylation,

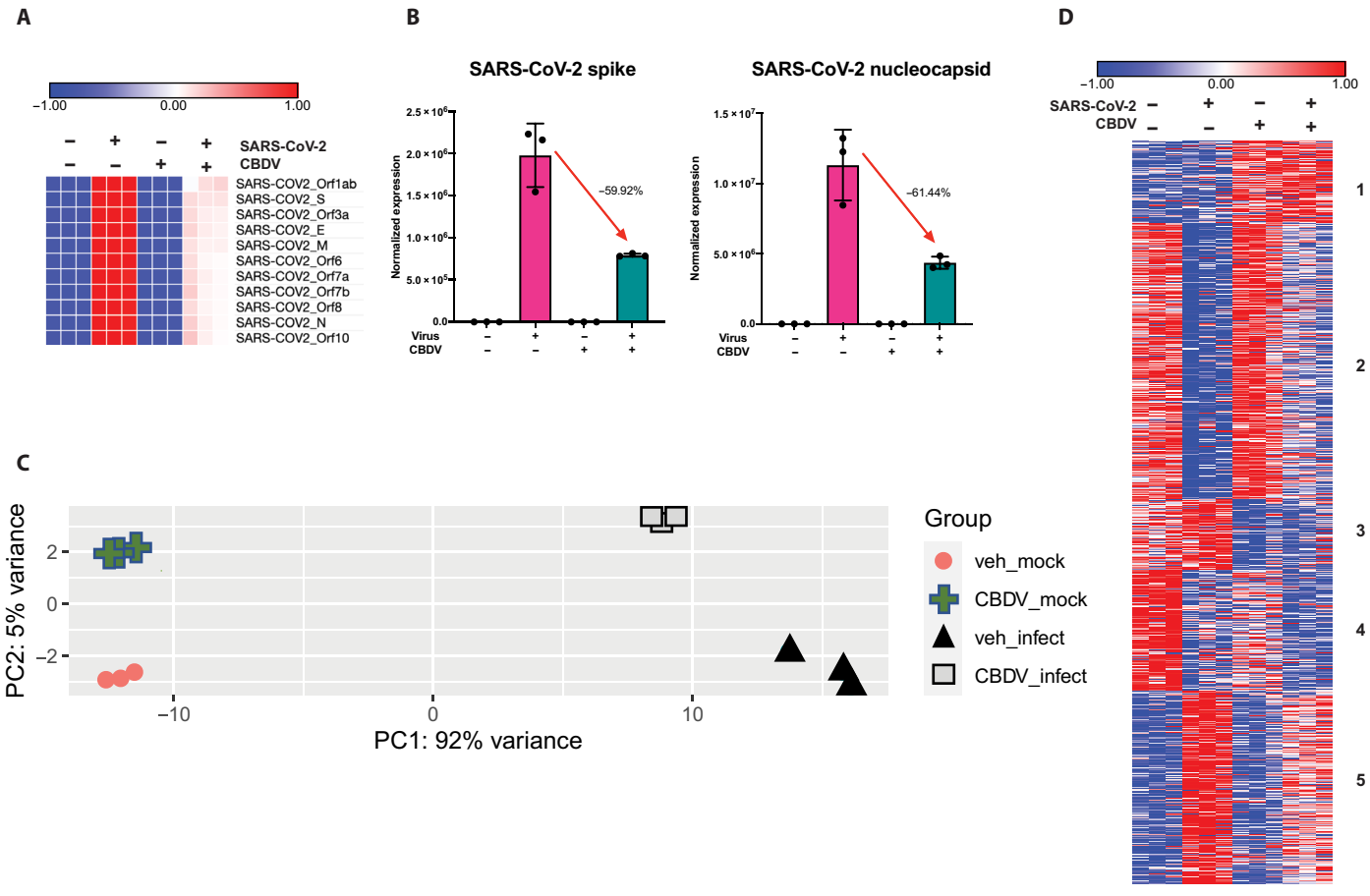

Fig. 5. Changes in viral and host cell transcription following SARS-CoV-2 infection or CBDV treatment. A549-ACE2 cells were infected with SARS-CoV-2 at an MOI of 3 with or without CBDV treatment at 10 μM for 24 hours. RNA-seq was performed as described in Materials and Methods. (**A**) Heatmap of relative levels of SARS-CoV-2 genes from the RNA-seq samples. (**B**) Expression levels of SARS-CoV-2 spike and nucleocapsid genes. Percent expression level changes for genes from infected cells compared to cells infected and CBD treated are indicated for each gene. (**C**) PCA of RNA-seq data showing control (veh_mock), SARS-CoV-2–infected (veh_infect), CBDV-treated (CBDV_mock), and SARS-CoV-2–infected plus CBDV–treated (CBDV_infect) samples. The first and second principal components (PC1 and PC2) of each sample are plotted. (**D**) Heatmap of normalized expression levels of 5000 most variable genes across all RNA-seq samples, clustered into six groups based on differential expression between treatment conditions.

which allosterically activates its RNase to initiate productive splicing of X-box binding protein 1 (XBP1) mRNA. Spliced XBP1 encodes a transcription factor that up-regulates many host stress responses, including ER chaperone induction and ER-associated degradation components (Fig. 6E) (*22*).

CBD strongly activates IRE1α RNase activity as shown by analysis of XBP1 splicing using both RNA-seq data to quantify spliced XBP1 as well as direct confirmation by qRT-PCR (Fig. 6B and fig. S15). As predicted, CBD induced XBP1 splicing in the presence or absence of virus, whereas CBDV had no significant effect and is comparable to virus alone. The time course and dose response curves for CBD induction of XBP1 splicing in the absence of the virus were consistent with the time course and dose responses for CBD inhibition of viral spike protein expression in A549-ACE2 cells (Fig. 6C). Furthermore, while an IRE1α knockout had no significant effect on SARS-CoV-2 infection, it shifted the dose response and significantly reduced the antiviral effects of CBD, leading to an approximately twofold increase in its EC_{50} against SARS-CoV-2 (Fig. 6D and fig. S16). Together, these results indicate that CBD induction of IRE1α is a critical component of its antiviral action against SARS-CoV-2.

CBD induces interferon expression as part of its antiviral activity

Another mechanism by which CBD could suppress viral infection and promote degradation of viral RNA is through induction of the interferon signaling pathway. Interferons are among the earliest innate immune host responses to pathogen exposure (*23*). As reported (*24*), SARS-CoV-2 infection suppresses the interferon signaling pathway (Fig. 7A and fig. S17). Many genes in the pathway such as interferon-stimulated gene 15 (ISG15), interferon induced protein with tetratricopeptide repeats 1 (IFIT1), IFIT3, suppressor of cytokine signaling 1 (SOCS1), and 2'-5'-oligoadenylate synthetase 1 (OAS1), an interferon-induced gene that leads to activation of RNase L and RNA degradation (*25*), were moderately up-regulated by CBD alone but highly induced by CBD in the presence of the virus (Fig. 7A and figs. S18 and S19). These latter results are consistent with the possibility that CBD sufficiently lowers the

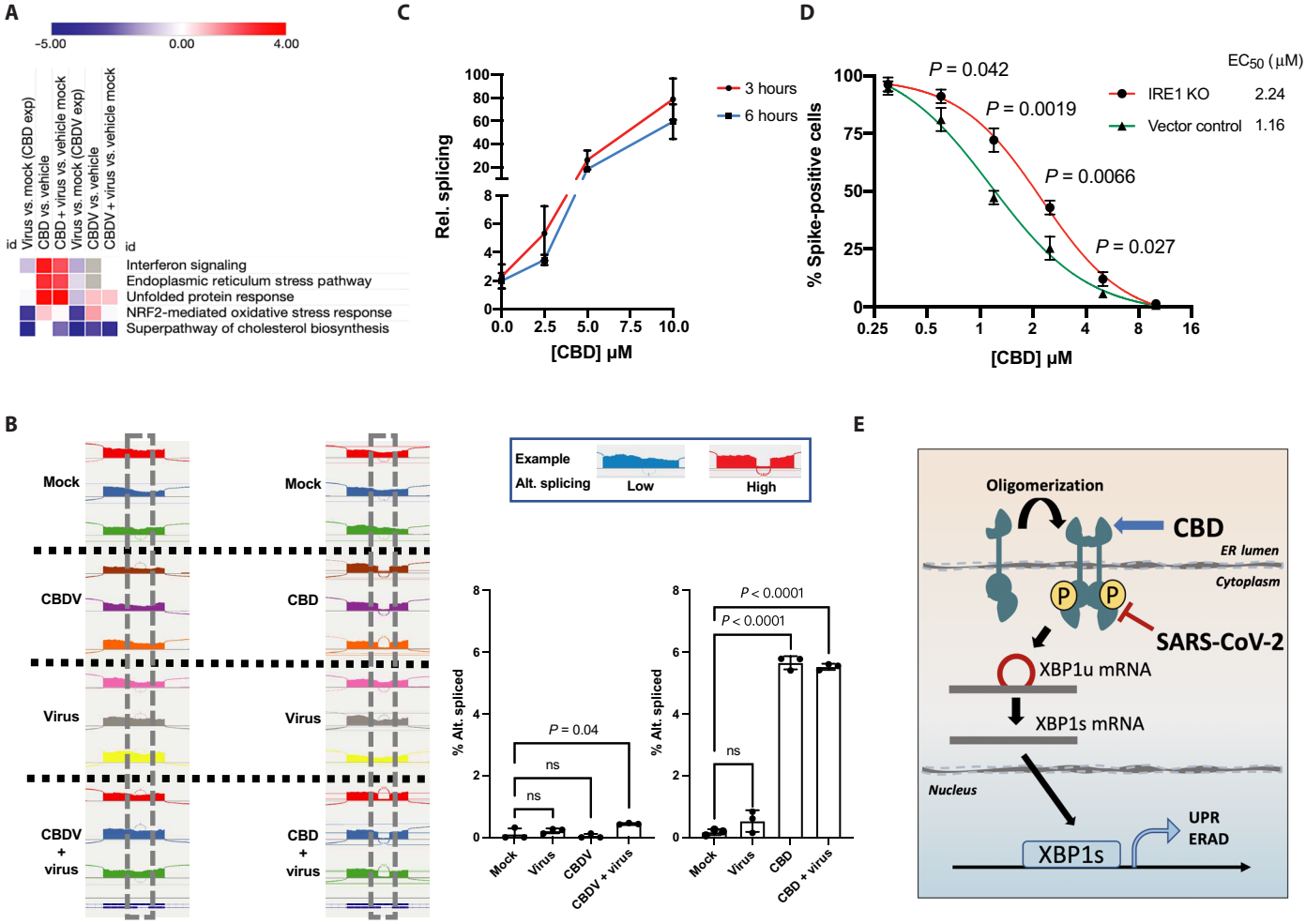

Fig. 6. CBD promotes host cell ER stress responses and IRE1α/XBP1 splicing, and IRE1α contributes to antiviral CBD activity. A549-ACE2 cells were infected with SARS-CoV-2 at an MOI of 3 with or without CBD or CBDV treatment at 10 μM (A and B) or as indicated (C) for 24 hours (A and B) or as indicated (C). (**A**) Heatmap of predicted pathway activation based on Ingenuity analysis of activation *z* scores for each pathway and each comparison. Red: Pathway is activated. Blue: Pathway is inhibited. White: Pathway is unchanged. Gray: No prediction due to lack of significance. NRF2, nuclear factor erythroid 2-related factor 2. (**B**) Analysis of XBP1 splicing by the IRE1α RNase. Reads representing spliced or unspliced XBP1 were identified and quantified for cells that were mock-treated, SARS-CoV-2–treated, or treated with CBD or CBDV either alone or in the presence of virus (left). Percentage of alternatively spliced reads for the RNA-seq samples were plotted, and unpaired *t* tests were performed comparing each experiment's mock samples to other samples (right). ns, not significant. (**C**) A549-ACE2 cells were treated by indicated concentrations of CBD for 3 and 6 hours. Relationship between CBD concentration and XBP1 splicing was determined by qRT-PCR. (**D**) Effect of IRE1α on dose response for antiviral activity of CBD. A549-ACE2 or A549-ACE2 cells lacking IRE1α (IRE1 KO) were treated with indicated doses of CBD, followed by infection with SARS-CoV-2 at an MOI of 0.5 for 48 hours. The cells were stained for spike protein, and the percentage of cells expressing the spike protein in each condition was plotted. EC_{50} values are indicated. Unpaired *t* tests were performed at each concentration and significant *P* values were shown. This is representative of three independent experiments (composite EC_{50} 1.7 versus 1.2, $P < 0.05$). (**E**) Schematic illustrating effect of CBD and SARS-CoV-2 on IRE1α RNase activity and XBP1 splicing. ERAD, ER-associated degradation.

effective viral titer to enable normal host activation of the interferon pathway. At the same time, CBD effectively reversed viral induction of cytokines that can lead to the deadly cytokine storm at later stages of infection (Fig. 7B). By contrast, the inactive homolog CBDV does not significantly induce genes within the interferon pathway or prevent cytokine induction (Figs. 6A and 7, A and C; and figs. S20, A and B, and S21).

To directly test the possibility that interferons might account in part for the antiviral activity of CBD, we exposed ACE2-A549 cells to a mixture of antibodies against type I (α, β, and ο) and type II (γ) interferons before 2.5 μM CBD treatment and viral infection. The results show that the anti-interferon antibodies reduce the antiviral effects of CBD and partially rescue SARS-CoV-2 infection (Fig. 7D). Collectively, these results suggest that CBD inhibits SARS-CoV-2 infection in part by activating IRE1α and the interferon pathways, leading to degradation of viral RNA and subsequent viral-induced changes in host gene expression, including cytokines.

CBD treatment significantly inhibits SARS-CoV-2 replication in mice

As several agents including cationic amphipathic drugs block SARS-CoV-2 replication in cultured cells but not in vivo (*26*), we determined whether CBD reduces viral titer in female K18-hACE2 mice (*27*). Mice were injected intraperitoneally twice daily with CBD

Table 1. Induction of PERK, IRE1, or ATF6 gene expression and function in response to CBD and/or SARS-CoV-2 virus. RNA-seq gene expression data are used for GSEA on three GO terms: "PERK-mediated UPR," "IRE1-mediated UPR," and "ATF6-mediated UPR" (GO numbers 36498, 36499, and 36500). Normalized enrichment score is shown under the "GSEA NES" (gene set enrichment analysis normal enrichment score) column (higher score = more enrichment). Fold change for transcriptional expression differences between PERK, IRE1, and ATF6 is shown for each comparison under the "RNA-seq fold change" column.

Comparison	UPR branch	GSEA NES	RNA-seq fold change
CBD versus mock	PERK	1.43	2.46
	IRE1	1.38	2.29
	ATF6	ND*	1.40
Virus versus mock	PERK	1.92	1.85
	IRE1	Not enriched	2.67
	ATF6	ND*	0.91
CBD + virus versus mock	PERK	1.45	3.24
	IRE1	1.44	2.76
	ATF6	ND*	1.24

*ND, not determined because of not enough genes to get reliable values.

(20 or 80 mg/kg) for 7 days before intranasal challenge with SARS-CoV-2 [2×10^4 plaque-forming units (PFU)]. After the challenge, administration of CBD continued twice daily for an additional 4 days (Fig. 8A). CBD treatment significantly inhibited viral replication in lungs and nasal turbinates at day 5 after infection in a dose-dependent manner (Fig. 8, B and C). The lower dose of CBD reduced viral load by 4.8-fold in lungs and 3.7-fold in nasal turbinates, while the higher dose decreased viral titers by 40- and 4.8-fold in lungs and nasal turbinates, respectively. During this period, the mice showed no signs of clinical disease, and their body weights were not significantly changed (Fig. 8D). These results establish the preclinical efficacy of CBD as an antiviral drug for SARS-CoV-2 during early stages of infection.

CBD is negatively associated with indications of SARS-CoV-2 infection in patient medical records

Given that high-purity CBD preparations are taken by a large number of individuals, we examined whether medication records of CBD prescriptions or use are associated with indications of SARS-CoV-2 infection (i.e., positive COVID-19 tests and/or COVID-19 diagnoses proximal to COVID-19 tests). An oral solution of CBD (100 mg/ml) (CBD100) is often used for the treatment of seizures (see the Patient Data Analysis Supplement). Analysis of 1212 patients from the National COVID Cohort Collaborative (N3C) (*28*) with a history of seizure-related conditions and a medication record of CBD100 revealed 6.2% (75 patients) with an indication of SARS-CoV-2 infection proximal to the dates of their first COVID-19 test in their N3C data. This was a significantly lower rate than the rates of matched control groups of patients that did not have any CBD100 records [e.g., 6.2% for CBD100 patients compared to 8.9% for non-CBD100 patients, $P = 0.014$; multivariable logit model odds ratio (OR) of 0.65, $P = 0.009$, 95% confidence interval (CI) (0.47 to 0.90)]. The demographics and medical history of the CBD100 patients were similar to those of the matched control group. The medical condition history for these patients included seizure-related conditions, the Centers for Disease Control (CDC) list of at-risk conditions (*29*) and other potential confounders such as conditions of reduced mobility, chronic pain, or developmental disabilities that can limit public interaction and COVID-19 exposure. The negative association was even more significant in analyses of a subgroup of 531 CBD100 patients who were likely taking CBD100 on the dates of their first COVID-19 tests [e.g., 4.9% among these CBD100 patients compared to 9.0% among 531 matched controls, $P = 0.011$; OR = 0.48, $P = 0.006$, 95% CI (0.29,0.81)] (Fig. 9 and table S4 in the Patient Data Analysis Supplement, which describes the patient data analysis methods and findings in detail).

DISCUSSION

Our results suggest that CBD and its metabolite 7-OH-CBD can block SARS-CoV-2 infection at early and even later stages of infection. The mechanism appears to be mediated, in part, by activation of the IRE1α RNase and interferon pathways. In addition to these cell-based findings, preclinical studies show that CBD treatment reduced viral titers in the lungs and nasal turbinates of SARS-CoV-2–infected mice. Last, analysis of a national sample of patients with active records of CBD100 consumption at the time of COVID testing revealed an association with substantially fewer SARS-CoV-2–positive test results. This negative association was robust to many sensitivity analyses, including changes in the matching and outcomes models, and merits further research into the potential of CBD to combat SARS-CoV-2 infection, such as validation in other large, multisite electronic health record datasets or prospective experimental designs.

One mechanism contributing to the antiviral activity of CBD is the induction of the interferon pathway both directly and indirectly following activation of the host immune response to the viral pathogen. Interferons have been tested clinically as potential treatments for COVID-19 (*30*). When hyperactivated by severe ER stress, IRE1α's RNase activity leads to the endonucleolytic decay of many ER-localized mRNAs [regulated IRE-1 dependent decay (RIDD)] and subsequent activation of RIG-I (retinoic acid-inducible gene I) and interferons (*18*). Although SARS-CoV-2 induces the kinase activity of IRE1α, it does not activate its RNase activity as monitored by XBP1 splicing. Thus, the RNase activity of IRE1α induced by CBD can potentially account for both the degradation of viral RNA and the induction of interferons by the RNA fragments. Further investigation will be

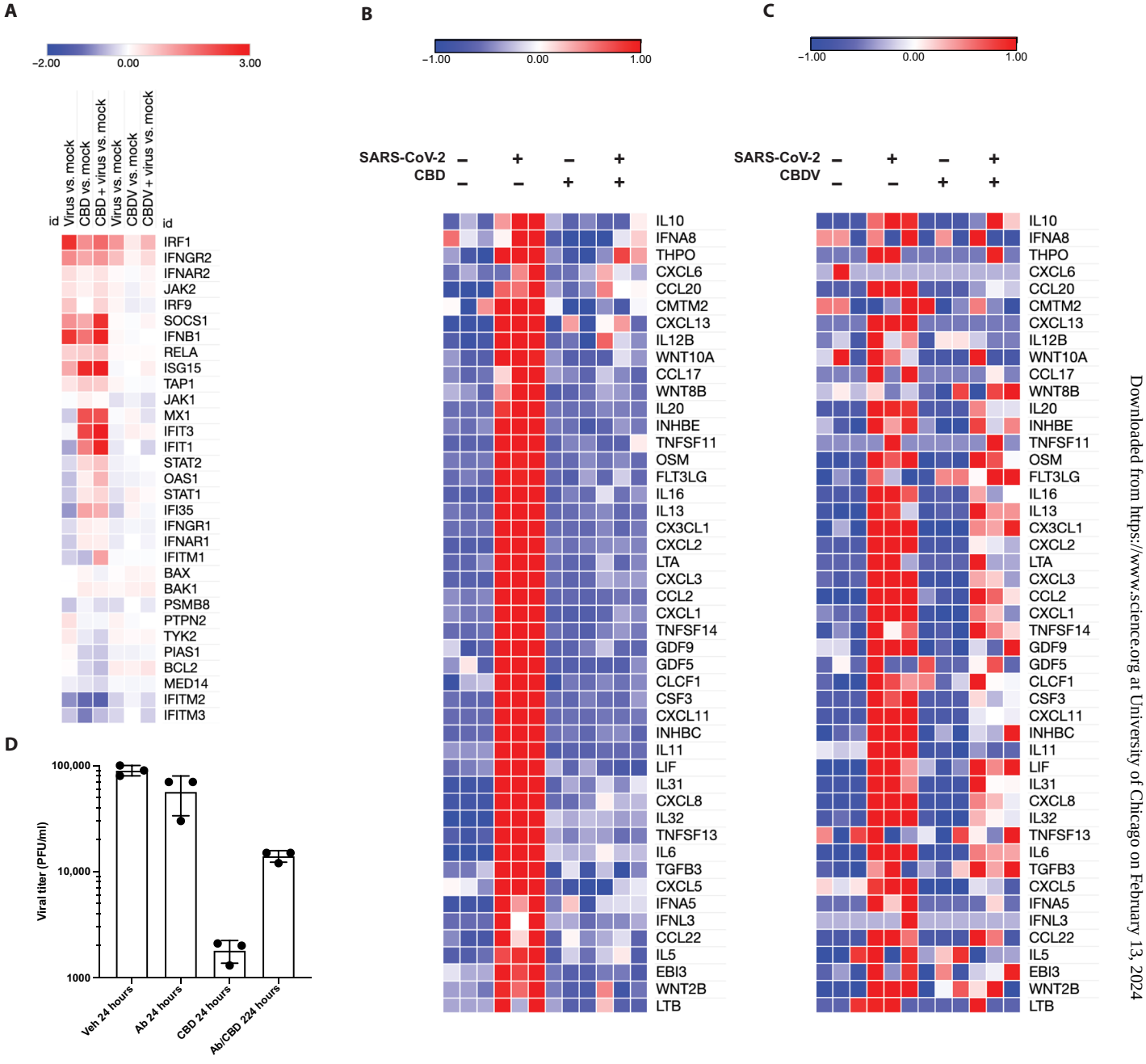

Fig. 7. CBD promotes host cell interferon responses and inhibits viral induction of cytokines. (**A**) Heatmap of fold change (log2) of genes from the Interferon Response Canonical Pathway for all virus- or CBD-treated samples compared to mock-treated samples. Columns 1 to 3 use samples from the RNA-seq experiment on CBD and SARS-CoV-2. Columns 4 to 6 use samples from the RNA-seq experiment on CBDV and SARS-COV-2. (**B**) Heatmap of normalized expression levels of GO Cytokine Activity genes that were up-regulated by the viral infection but down-regulated by CBD treatment for all RNA-seq samples from the experiment on CBD and SARS-CoV-2. (**C**) Heatmap of the normalized expression levels of the same genes for all RNA-seq samples from the experiment on CBDV and SARS-CoV-2. (**D**) A549-ACE2 cells were treated with 2.5 μM vehicle or CBD with or without Human IFN-γ Antibody and Human Type I IFN Neutralizing Ab Mixture at 2 hours before infection. Cells were then infected with 0.5 MOI SARS-CoV-2 and incubated for 24 hours, and active virus was measured using a plaque assay. The results are representative of three independent experiments. PFU, plaque-forming units.

required to determine whether both antiviral effects of CBD are linked to the ER stress response. CBD also suppresses cytokine activation in response to viral infection, reducing the likelihood of immune cell recruitment and subsequent cytokine storms within the lungs and other affected tissues. These results complement previous findings suggesting that CBD suppresses cytokine production in recruited immune cells such as macrophages (*31*). Thus, CBD has to the potential not only to act as an antiviral agent at early stages of infection but also to protect the host against an overactive immune system at later stages.

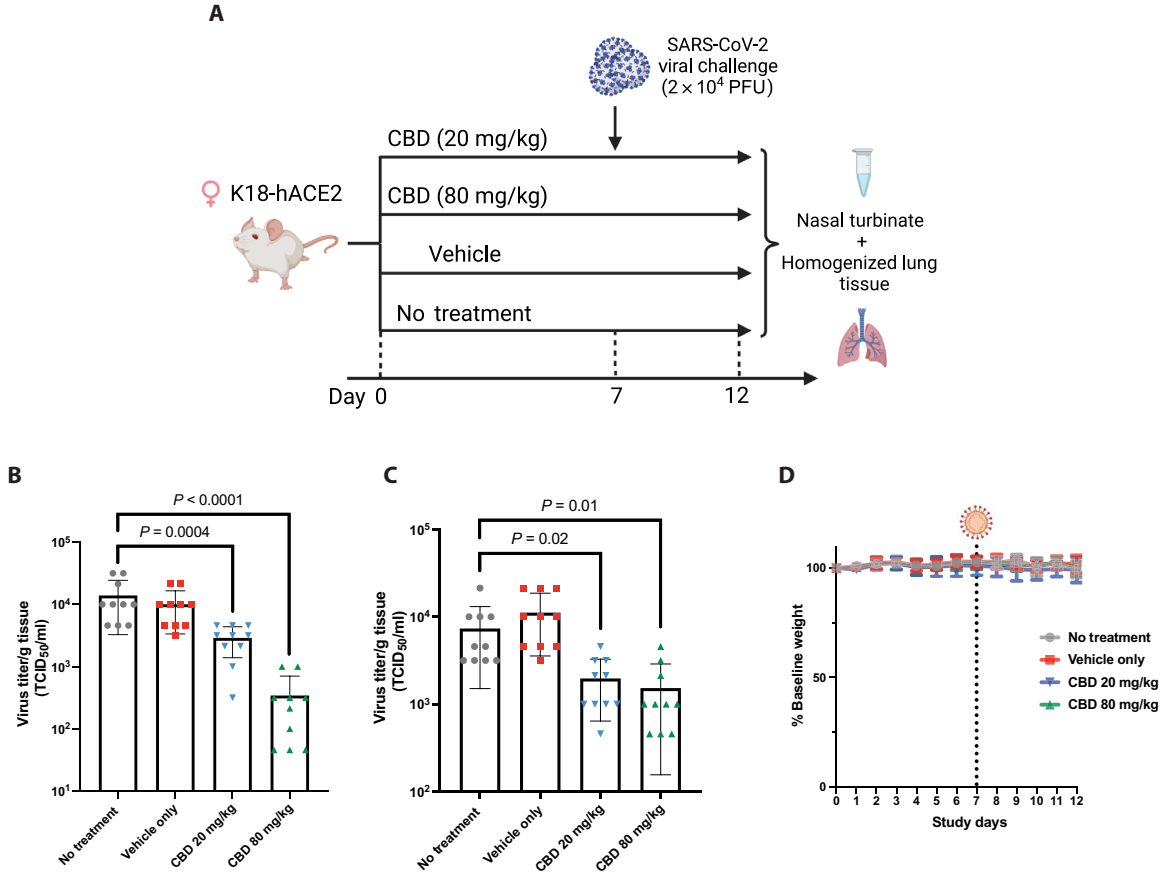

Fig. 8. CBD inhibits SARS-CoV-2 replication in mice. (**A**) Timeline of the mouse experiment. (**B**) Viral titer in lungs from all animals measured 5 days after viral challenge (day 12). $TCID_{50}$, median tissue culture infectious dose. (**C**) Viral titer in nasal turbinates from all animals measured 5 days after viral challenge (day 12). (**D**) Weight measurements of mice in each treatment group ($n = 10$) during the study. The body weight of each mouse is normalized to its weight measured at day 0. All animals were challenged with SARS-CoV-2 by intranasal instillation at day 7.

CBD has a number of advantages as a potential preventative agent against SARS-CoV-2. CBD as a food additive with THC content less than 0.3% is widely available without restricted access. With proper formulation, quality control, and delivery, CBD could be used prophylactically in contrast to recent antiviral drugs. Multiple means of CBD ingestion are possible, including potential for inhalation and nasal delivery. CBD blocks viral replication after entry into cells and thus is likely to be effective against viral variants with mutant spike proteins. Unlike drugs such as remdesivir or antiviral antibodies, CBD administration does not require injection in hospital settings. Last, CBD is associated with only minor side effects (*32*).

However, several issues require close examination before CBD can be considered further or even explored as a therapeutic lead for COVID-19 (*12*). Although many CBD and CBD-containing products are available on the market, they vary vastly in quality, CBD content, and their pharmacokinetic properties after oral administration, which are mostly unknown. CBD is quite hydrophobic and forms large micellar structures that are trapped and broken down in the liver, thereby limiting the amount of drug available to other tissues after oral administration. Inactive carriers and formulation adjuvants have a significant impact on clinically obtainable concentrations. As CBD is widely sold as a preparation in an edible oil, we analyzed flavored commercial hemp oils and found a CBD content of only 0.30% in a representative sample (fig. S22). The purity of CBD and the chemical composition of the materials labeled as CBD are also important, especially in light of our findings suggesting that other cannabinoids such as THC might act to counter CBD antiviral efficacy. This essentially eliminates the feasibility of marijuana serving as an effective source of antiviral CBD, in addition to issues related to its legal status. Last, other means of CBD administration such as vaping and smoking raise additional concerns about potential lung damage.

Future studies to explore the optimal means of CBD delivery to patients along with clinical trials will be needed to further evaluate the promise of CBD as a therapeutic to block SARS-CoV-2 infection. Our animal studies provide preclinical support for evaluation of CBD as an anti–SARS-CoV-2 therapeutic agent in clinical trials. We advocate carefully designed placebo-controlled clinical trials with known concentrations and highly characterized formulations to define CBD's role in preventing and treating early SARS-CoV-2 infection. The necessary human in vivo concentration and optimal route and formulation remain to be defined. We strongly caution against the temptation to take CBD in presently available formulations including edibles, inhalants, or topicals as a preventative or treatment therapy at this time, especially without the knowledge of a rigorous randomized clinical trial with this natural product (*33*).

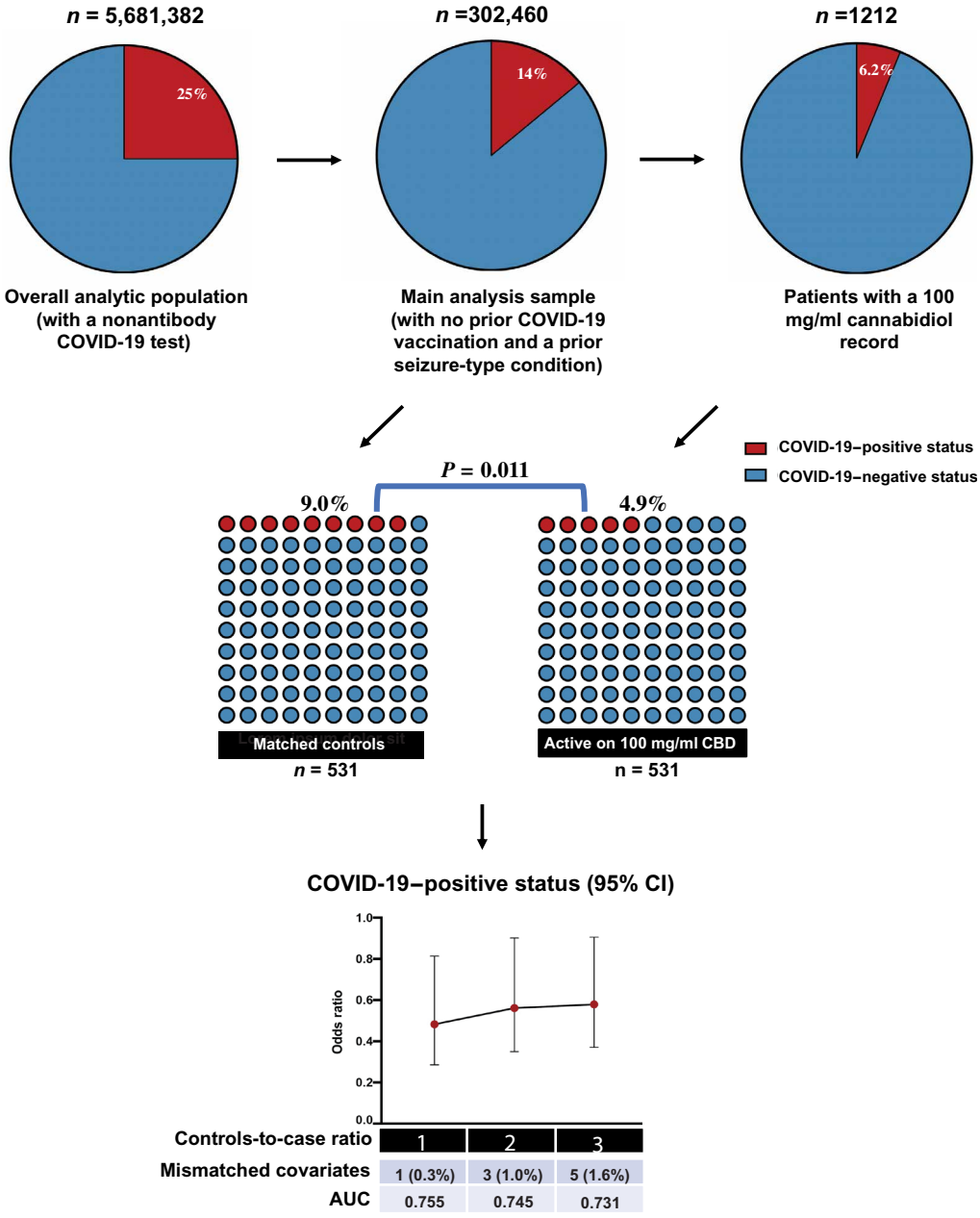

Fig. 9. CBD100 medication records in patients are significantly associated with less COVID-19 positivity. Schematic showing derivation of our main analysis sample and CBD patient groups obtained from the National COVID Cohort Collaborative (N3C). Successive analyses of patient subsets are illustrated. The final panel shows associations between having a CBD100 medication record on the date of their first COVID-19 test and COVID-19–positive status among matched control groups of increasing size (i.e., 1-to-1, 2-to-1, and 3-to-1 ratios of controls to CBD patients). A mismatched covariate has a standardized mean difference greater than 0.10 and a two-sided Fisher's exact test *P* value of less than 0.05 when comparing its distribution between the CBD patients and their matched controls. AUC refers to area under the receiver operating characteristic curve. Detailed information regarding the patient data analysis methods and findings is in the Patient Data Analysis Supplement.

MATERIALS AND METHODS

Study design

The goal of this study was to determine whether CBD, a natural product extracted from the cannabis plant, has the potential to inhibit infection of cells by SARS-CoV-2. To this end, we utilized three different human or monkey cell lines. We tested four independent preparations of CBD from chemical as well as natural sources and also tested related cannabinoid compounds and metabolites. We used RNA-seq analysis to demonstrate that CBD, in contrast to the inactive cannabinoid CBDV, effectively eliminated SARS-CoV-2 viral RNA from infected cells, activated the ER stress response and XBP1 splicing, induced expression of the interferon pathway, and suppressed viral induction of cytokines. We demonstrated using IRE1α knockout cells and anti-interferon blocking antibodies that both IRE1 and interferons contribute to the antiviral activity of CBD. Last, using medical records for groups of human patients from the

N3C under appropriate institutional review board (IRB) protocols, we analyzed the association of patients taking CBD with their risk of testing positive for SARS-CoV-2. Statistics are provided in the corresponding figures and in methods.

Materials, cells, and viruses

High-purity CBD was acquired from two chemical companies or two online commercial sources. 7-OH-CBD was purchased from Cerilliant Corporation (Round Rock, TX). All commercial compounds used were validated by NMR as described below. Cannabinoid-infused hemp oil containing more than 1500-mg cannabinoids was from Bluebird Botanicals (Louisville, CO, USA). Hemp extract from *C. sativa* biomass was from Hopsteiner Ltd. (Yakima, Washington, USA). Low-CBD hemp oil was obtained from an online commercial source. A549-ACE2 cells were provided by tenOever and colleagues (*24*). Vero E6 and Calu3 cells were purchased from the American Type Culture Collection (ATCC). SARS-CoV-2 [novel coronavirus (nCoV)/Washington/1/2020] was provided by N. Thornburg (CDC) via the World Reference Center for Emerging Viruses and Arboviruses (Galveston, TX) and from BEI Resources for the in vivo studies. SARS-CoV-2 variants were provided by BEI Resources. The α variant is BEI number NR-54000, isolate hCoV-19/England/204820464/2020 sourced from Public Health England. The β variant is BEI number 54009, B.1.351(20H/501Y.V2) sourced from the Africa Health Research Institute. The γ variant is BEI number 54982, isolate hCoV-19/Japan/TY7-503/2021 sourced from the Japan National Institute of Infectious Disease. Viral stocks were made by two passages in Vero E6 cells, and stock titers were determined by limiting dilution plaque titer on VeroE6 cells (described below).

SARS-CoV-2 infection assay

All SARS-CoV-2 infections were performed in biosafety level 3 conditions at the Howard T. Rickett Regional Biocontainment Laboratory, University of Chicago. In vivo infections were performed in animal biosafety level 3 conditions at the Center for Predictive Medicine for Biodefense and Emerging Infectious Diseases, the University of Louisville Regional Biocontainment Laboratory. Cells in Dulbecco's modified Eagle's medium (DMEM) + 2% fetal bovine serum (FBS) were treated with CBD or other inhibitors or 2 hours with twofold dilutions beginning at 10 μM in triplicate for each assay. A549-ACE2 cells were infected with an MOI (multiplicity of infection) of 0.5 in media containing the appropriate concentration of drugs. Vero E6 cells were infected with an MOI of 0.1 in media containing the appropriate concentration of drugs. After 48 hours, the cells were fixed with 3.7% formalin, blocked, and probed with mouse anti-spike antibody (GTX632604, GeneTex) diluted 1:1000 for 4 hours, rinsed, and probed with anti-mouse–horseradish peroxidase for 1 hour, washed, and then developed with 3,3′-diaminobenzidine substrate for 10 min. Spike-positive cells ($n > 40$) were quantified by light microscopy as blinded samples. Viral titers were determined by plaque assay. Briefly, a monolayer of E6 cells is infected with a series of serial dilutions of virus sample for 1 hour at 37°C. The viral inoculum is then removed and replaced by a minimum essential medium overlay containing 1.25% carboxymethyl cellulose. Cells are incubated for 72 hours after which overlay medium is removed, and cells are fixed with 10% formalin and stained with 0.25% crystal violet solution. Plaques are counted in the dilution well with between 10 and 100 plaques, and original concentration of viral sample is calculated. Data were analyzed and plotted using GraphPad Prism, and EC_{50} values were extracted from nonlinear fit of response curves.

Crystal violet toxicity assay

Cells were treated with varying concentrations of different compounds in 2% DMEM starting at 10 μM and going down by one-half for six more dilutions. Cells were incubated with the drug for 48 hours. Cells were fixed with 10% formalin solution for 30 min. Then, they were stained with 1% crystal violet solution for 30 min after which plates were dried and the amount of crystal violet staining was assessed by measuring absorbance at 595 nm on a Tecan M200 plate reader. Absorbance readings were normalized to those of the control wells not treated by the drug to measure the differences in cell growth with or without the drug treatment.

Spike protein and antibody neutralizing assay

A549-ACE2 cells were treated with 10 μM CBD either 2 hours before infection or 2, 6, or 15 hours after infection. Cells were infected with an MOI of 0.5 for 2 hours. Then, the infection medium was replaced with a medium containing CBD or dimethyl sulfoxide (DMSO), and the samples were incubated at 37°C for 16 hours. In one experiment when CBD was added 2 hours after infection, infection medium was replaced with CBD or DMSO and neutralizing antibody (Active Motif 001414). After 16 hours, the samples were fixed with 10% formalin and underwent immunohistochemistry for spike protein. Neutralizing antibody efficiency was tested by incubating 400 PFU of virus with or without 100 nM antibody at 37°C for 1 hour. Then, A549-ACE2 cells were infected with the mixture for 16 hours. Spike-positive cells were quantified as described above.

Interferon antibody neutralizing assay

A549-ACE2 cells were treated with 2.5 μM CBD, Human IFN-γ Antibody (1 μg/ml) (MAB285-100), and 1:25 dilution of Human Type I IFN Neutralizing Ab Mixture (PBL Assay Science, 39000-1) 2 hours before infection. Cells were then infected with 0.5 MOI and incubated for 24 hours, after which supernatants were collected and active virus was measured using the plaque assay described above.

Generation of IRE1α knockout cells by CRISPR-Cas9

Lentivirus stocks were by using lentiCRISPR v2 (Addgene) with single guide RNA targeting IRE1 sequence (CGGTCACTCACCCCGAGGCC). The infected A549-ACE2 cells were polyclonally selected and maintained using medium supplemented with puromycin (4 μg/ml) for 1 week.

Description of the cannabinoids

CBD can be procured by isolating CBDA from *C. sativa* plant material and then inducing chemical decarboxylation or via decarboxylation of cannabinoids contained in raw plant material or extract and subsequent isolation of CBD. CBDV is a naturally occurring CBD homolog that has an *n*-propyl in place of CBD's *n*-pentyl side chain. CBG, in the form of cannabigerolic acid, is the metabolic precursor to both tetrahydrocannabidiolic acid and CBDA in *C. sativa*. THC is a cyclized congener of CBD that is obtained after tetrahydrocannabinolic acid decarboxylation. THC is present in *C. sativa* in both Δ^9-*cis* and Δ^9-*trans* stereoisomers. CBC, in the form of cannabichromenic acid, represents a third possible cannbigerolic acid metabolite with a chromene ring in the geranyl residue.

Acquisition, isolation, and characterization of cannabinoids

In the present study, purification of CBD from natural sources used (i) cannabinoid-infused hemp oil containing 1500+-mg cannabinoids in medium-chain triglycerides per fluid ounce, manufactured by Bluebird Botanicals (Louisville, CO, USA) and (ii) hemp extract prepared by supercritical fluid extraction (SFE) with CO_2 from *C. sativa* biomass qualifying as hemp, manufactured by Hopsteiner Ltd. (Yakima, WA, USA) with a 54.7% total content of CBD, calculated as CBD + CBDa × 0.877. Typical purities of these CBD preparations are in the 90 to 97% range including foreign impurities (e.g., residual solvent) determined by quantitative ^{1}H NMR (qHNMR). Details of the purification and structure analysis methodologies are detailed in a concurrent publication, which is currently in press (*Journal of Natural Products*). In brief, the methodologies can be summarized as follows:

Purification procedure

CBD, CBC, CBG, Δ^9-*trans*-THC, Δ^9-*cis*-THC, and CBDV were isolated from the hemp oil and CBDA from the crude hemp SFE extract, using centrifugal partition chromatography, a countercurrent separation technique, and a biphasic liquid-liquid solvent system.

Structure elucidation methodology

The identities of the commercially sourced CBD and other cannabinoid samples were verified by one-dimensional (1D) ^{1}H NMR analysis, performed as qNMR measurement, via comparison with an authentic HiFSA profile of CBD as published (*12*). In addition to an overall excellent match of the profiles, the highly coupled fingerprint signal of H-4"ax served as a highly specific identity marker. The structures of the cannabinoids that were sourced commercially or purified from the natural sources were established by a combination of 1D/2D NMR and liquid chromatography–high-resolution mass spectrometry analysis, taking into account reference data from the literature.

NMR sample preparation

For commercial samples supplied as solution, the solvent was removed carefully in vacuo and 450 µl of deuterated methanol (MeOH-d_4) added to the residue using a precision syringe. The solution was transferred into a 5-mm NMR tube with a glass pipette, the vial was rinsed three times with 25 µl of solvent, and the rinsing solution was transferred into the same NMR tube, for a final volume of 525 µl. Commercial and isolated samples available as solids were directly weighed into a 5-mm NMR tube, and 500 µl of solvent was added with a precision syringe. For analysis of the commercial hemp oil preparation, 10 drops (0.25 ml equivalent to 14 to 15 drops) was added into the 5-mm NMR tube directly. The net weight of hemp oil in the NMR tube was 198.50 mg, determined on a 0.01-mg precision balance, and 0.90 mg of dinitrobenzoic acid was added as an internal calibrant for internal calibration (IC)–qHNMR; 325 µl of $CDCl_3$ and 10 µl of CD_3OD were added, and the tube was flame-sealed.

NMR data acquisition and processing and qNMR evaluation

The NMR spectra were acquired on Jeol 600 ECZ-600R (with HFX Royal RT probe) and Bruker 600 Avance III (^{13}C direct He cryogenic probe) two-channel spectrometers. For qHNMR measurements, time domain was set to 64k, relaxation delay (D1) was 60 s, and 90° excitation pulses were used for a total of 32 signal-averaged scans. The receiver gain (RG) was 32 for all samples, except for one mass-limited sample < 1 mg (RG = 101) and the large-quantity hemp oil sample (RG = 2; 15° excitation pulse used). Determination of sample purity and CBD content in hemp oil by qNMR was performed using the 100% qNMR approach and openly published worksheets (https://gfp.people.uic.edu/qnmr/content/qnmrcalculations/100p.html). The qNMR purity of all CBD samples was >97% including foreign impurities, and no cannabinoid congeners could be detected at levels above 1.0%. Using the absolute qHNMR method with IC (IC abs-qNMR), the content of CBD in hemp oil was determined as 0.30%.

Pseudotyped lentivirus production

293 T and 293 T–ACE2 cells were cultured in DMEM (Corning, 10017CV) with 1× sodium pyruvate (Gibco, 11360070) and 10% FBS (HyClone, SH30910). Lentivirus particles pseudotyped with SARS-CoV-2 (Wuhan-Hu-1) spike protein or VSV-G were generated as described (*19*). Briefly, 293 T cells were transfected using TransIT-LT1 (Mirus) with third-generation lentivirus packaging vectors (HDM-Hgpm2, HDM-tat1b, and pRC-CMV-Rev1b), transfer vector (pHAGE-CMV-ZsGreen-W) and either SARS-CoV-2 spike (HDM-IDTSpike-fixK) or VSV-G (HDH-VSVG). Supernatants collected at 36 and 60 hours after transfection were pooled, syringe-filtered, and frozen in single-use aliquots at −80°C. All plasmids used for lentivirus production were provided by J. Bloom (University of Washington, Seattle).

Pseudovirus binding assay

293 T–ACE2 cells were seeded at 1.2×10^4 cells per 96 wells in black-wall, clear-bottom plates. The next day, twofold dilutions of CBD stock (10 mM) were prepared in DMSO, followed by 1:1000 dilutions in either complete DMEM or pseudovirus preparation. SARS-CoV-2 spike pseudovirus was used undiluted, while VSV-G pseudovirus was diluted 1:1500 in complete DMEM. Cells and pseudovirus were pretreated with CBD dilutions for 2 hours and 1 hour at 37°C, respectively. Cells were infected with pseudovirus for 72 hours, fixed with 4% paraformaldehyde, stained with a nuclear marker (Hoechst 33342, Thermo Fisher Scientific, H3570) and imaged. 293 T–ACE2 cells were supplied by J. Bloom (University of Washington, Seattle).

Pseudovirus neutralization assay

293 T or 293 T–ACE2 cells were seeded at 1.2×10^4 cells per 96 wells in black-wall, clear-bottom plates. The next day, SARS-CoV-2 spike neutralizing antibody (Sino Biological, 40592-R001) was diluted in complete DMEM to a starting final concentration of 300 ng/100 µl per 96 wells, followed by subsequent threefold dilutions. The neutralizing antibody was incubated with pseudovirus for 1 hour at 37°C. Cells were infected with pseudovirus with or without neutralizing antibody for 72 hours, fixed with 4% paraformaldehyde, stained with nuclear marker Hoechst 33342, and imaged.

Protease inhibition assay

Assays were performed in duplicate at room temperature in 96-well black plates at 25°C. Reactions containing varying concentrations of inhibitor (10 or 50 µM) and 3CLpro enzyme (0.4 µM) or PLpro enzyme (0.3 µM) in tris-HCl (pH 7.3) and 1 mm EDTA were incubated for approximately 5 min. 3CLpro reactions were then initiated with TVLQ-methyl-amino coumarin (AMC) probe substrate (40 µM), and PLpro reactions were initiated with LKGG-AMC probe substrate (40 µM). The reaction plate was shaken linearly for 5 s and then measured for fluorescence emission intensity (excitation λ,

364 nm; emission λ, 440 nm) over time (1 min to 3 hours) on a Synergy Neo2 Hybrid). Each assay contained two to three positive control wells (DMSO) and two negative control wells (assay components without protease). Data were normalized to the positive control wells at 3 hours, which were assigned an arbitrary value of 100.

Immunoblotting

A549-ACE2 cells were treated with CBD, treated with vehicle (DMSO) only, or left untreated for 24 hours. Cells were first washed with ice-cold phosphate-buffered saline (PBS). Whole-cell extraction were prepared by directly lysing cells with Laemmli sample buffer (Bio-Rad, 1610747) supplemented with protease inhibitor (Roche, 4693159001), phenylmethylsulfonyl fluoride (Roche, 10837091001), and phosphatase inhibitor (GB-450) at 4°C. Protein samples were lastly boiled at 98°C for 5 min. Western blotting was performed using antibodies for ACE2 (Abcam, 108252) and α-tubulin (Invitrogen, MA1-19401) for control. For validations of IRE1α knockout in A549-ACE2, cells, antibodies for IRE1α (Cell Signaling Technology, 3294S) and glyceraldehyde-3-phosphate dehydrogenase (Cell Signaling Technology, 5174S) were used. Blots were imaged and quantified using Li-COR Odyssey Fc.

RNA sequencing

Lung alveolar A549 cells were stably overexpressed with human ACE2 protein and seeded at 10,000 cells per well in a 96-well plate. CBD or vehicle was added together to the cells. CBD (Cayman Chemical, 90080) was dissolved in a 10 mM stock solution with DMSO (100 ml; Sigma-Aldrich, D2650). The final concentration of CBD was 10 μM. The virus stock was then removed and replaced with fresh 2% FBS-DMEM media with drug. The cells were incubated for another 24 hours before total RNA extraction using the NucleoSpin 96 RNA kit (Takara Bio, 740709). Three independent biological replicates were performed per experimental condition, with 12 total RNA samples. RNA sample quality check, library construction, and sequencing were performed by the University of Chicago Genomics Facility following standard protocols. The average RNA Integrity Score was 8.9. All 12 samples were sequenced in two runs by a NovaSeq 6000 sequencer to generate paired-end 100–base pair reads. For each sample, the raw FASTQ files from two flow cells were combined before downstream processing. CBDV was isolated from the hemp oil as described above, and identical studies as those described above with CBD were performed. The average RNA Integrity Score for the CBDV samples was also 8.9.

RNA-seq data for both CBD and CBDV-treated cells were analyzed separately using a local Galaxy 20.05 instance for the following steps (*34*). Quality and adapter trimming were performed on the raw sequencing reads using Trim Galore! 0.6.3 (*35*). The reads were mapped to both the human genome (UCSC hg19 with GENCODE annotation) and the SARS-COV-2 genome (NCBI Assembly ASM985889v3 with Ensembl annotation) using RNA STAR 2.7.5b (*36*). The resulting mapped reads from each sample were counted by featureCounts 1.6.4 (*37*) to generate per-gene read counts. The raw counts were analyzed for differential expression between experimental conditions using DESeq2 1.22.1 (*38*), which also generated a normalized gene expression matrix and a PCA plot of the samples.

The number of alternatively spliced XBP1 reads was counted by Integrative Genomics Viewer 2.9.4 (*39*) using aligned reads data from RNA STAR (see above). The total number of XBP1 reads was counted by featureCounts as above. For each sample, the relative XBP1 splicing was determined by dividing the reads containing the alternative splicing site by the total XBP1 reads.

Quantitative reverse transcription polymerase chain reaction

Complementary DNA (cDNA) was synthesized from RNA samples using the High-Capacity cDNA Reverse Transcription Kit (Thermo Fisher Scientific, 4368813). cDNA samples were diluted in molecular biology–grade water, and qRT-PCR experiments were performed on a Roche LightCycler 96 Instrument using the Applied Biosystems PowerUp SYBR Green Master Mix (Thermo Fisher Scientific, A25776). Results were analyzed by the Roche LightCycler 96 Software. Ribosomal protein L13a (RPL13A) was used as a reference gene. The following primer pairs were used:

ERN1, CCGAACGTGATCCGCTACTTCT (forward) and CGCAAAGTCCTTCTGCTCCACA (reverse); EIF2AK3, GTCCCAAGGCTTTGGAATCTGTC (forward) and CCTACCAAGACAGGAGTTCTGG (reverse); ATF6, CAGACAGTACCAACGCTTATGCC (forward) and GCAGAACTCCAGGTGCTTGAAG (reverse); IFIT1, GCCTTGCTGAAGTGTGGAGGAA (forward) and ATCCAGGCGATAGGCAGAGATC (reverse); IFIT3, CCTGGAATGCTTACGGCAAGCT (forward) and GAGCATCTGAGAGTCTGCCCAA (reverse); ISG15, CTCTGAGCATCCTGGTGAGGAA (forward) and AAGGTCAGCCAGAACAGGTCGT (reverse); OAS1, AGGAAAGGTGCTTCCGAGGTAG (forward) and GGACTGAGGAAGACAACCAGGT (reverse);

SOCS1, TTCGCCCTTAGCGTGAAGATGG (forward) and TAGTGCTCCAGCAGCTCGAAGA (reverse); alternatively, spliced XBP1, GCTGAGTCCGCAGCAGGT (forward) and CTGGGTCCAAGTTGTCCAGAAT (reverse); total XBP1, TGAAAACAGAGTAGCAGCTCAGA (forward) and CCCAAGCGCTGTCTTAACTC (reverse); and RPL13A, CTCAAGGTGTTTGACGGCATCC (forward) and TACTTCCAGCCAACCTCGTGAG (reverse).

Clustering of variable genes

The top 5000 most variable genes were selected, and the normalized gene expression data were analyzed by the Morpheus software (https://software.broadinstitute.org/morpheus). *K*-means clustering with six clusters was applied to the gene expression data of the RNA-seq experiment involving CBD and SARS-CoV-2, and *K*-means clustering with five clusters was applied to the gene expression data of the RNA-seq experiment involving CBDV and SARS-CoV-2. For each gene, the normalized expression values of all samples were transformed by subtracting the mean and dividing by the SD. The transformed gene expression values were used to generate the heatmap.

XBP1 splicing assay

qRT-PCR was used to quantify relative expression of spliced version of XBP1 (XBP1s) using specific pairs of primers for human alternatively spliced XBP1 and total XBP1 (primer sequences are described above) as previously described (*40*). Relative percentage of alternative splicing of XBP1 (%XBP1s) was indicated by calculating the ratio of signals between XBP1s and total XBP1.

Ingenuity Pathway Analysis

Expression data ($\log_2$ fold change) and predicted activation status of genes were overlaid onto the interferon signaling pathway and

the ER stress pathway maps using Ingenuity Pathway Analysis (IPA). Figures were generated through the use of IPA (QIAGEN Inc). Normalized gene expression values or fold change (log_2) of genes were analyzed by the Morpheus software. For each gene, the normalized expression values of all samples were transformed by subtracting the mean and dividing by the SD. The transformed gene expression values were used to generate the heatmaps. IPA-predicted activation *z* scores of relevant pathways from the RNA-seq data were also graphed by the Morpheus software.

Gene set enrichment analyses

To identify themes across the six clusters, functional GSEAs for the genes in each cluster were performed using Metascape (*41*). The following categories were selected for the enrichment analyses: Gene Ontology (GO) Molecular Functions, Kyoto Encyclopedia of Genes and Genomes (KEGG) Functional Sets, GO Biological Processes, Canonical Pathways, and KEGG Pathway. Additional parameters for Metascape: minimum overlap = 3, *P* cutoff = 0.05, minimum enrichment = 1.5. To identify gene sets in which activities were reversed by CBD with viral infection, the input gene list includes genes significantly down-regulated by the virus [differential expression comparing vehicle-infect (veh_infect) versus vehicle-mock (veh_mock), *q*-value cutoff of 0.01], while also significantly up-regulated by CBD (differential expression comparing CBD_infect versus veh_infect, *q*-value cutoff 0.01). A second list includes genes significantly up-regulated by the virus (differential expression comparing veh_infect versus veh_mock) while also significantly down-regulated by CBD (differential expression comparing CBD_infect versus veh_infect). GSEAs were performed on these two lists of genes using the same Metascape method. The same analyses were also performed on the differential expression data from RNA-seq experiments involving CBDV and SARS-CoV-2 with a *q*-value cutoff of 0.05. GSEA v4.1.0 was used to perform specific GSEAs on GO terms PERK-mediated UPR and IRE1-mediated UPR using the differential expression data from the RNA-seq experiment involving CBD and SARS-CoV-2 (*42*, *43*).

CBD treatment and SARS-CoV-2 challenge in mice

Nine- to 11-week-old female K18-hACE2 mice (*27*) were purchased from The Jackson Laboratory (stock no. 034860). Following acclimation, mice received CBD treatment (20 or 80 mg/kg) via twice daily intraperitoneal injection in a volume of 0.1 ml. The injection solution was prepared immediately before each treatment. First, the CBD powder from supplier D was dissolved in 100% ethanol. Then, the CBD solution was mixed with Cremophor EL (Millipore Sigma, 238470), followed by PBS solution at a ratio of 1:1:18. The vehicle injection solution was prepared by mixing 100% ethanol, Cremophor EL, and PBS at a 1:1:18 ratio. For each injection, the final amount of CBD was either 20 or 80 mg/kg of mouse body weight depending on treatment group. Control groups were treated with vehicle only or received no treatment. Following 7 days of treatment, all animals were anesthetized and challenged with 2×10^4 PFU of SARS-CoV-2 (nCoV/Washington/1/2020) via intranasal instillation in a volume of 0.05 ml. After challenge, CBD treatment continued twice daily for an additional 4 days. Mice were also monitored twice daily for the development of clinical disease. Body weights were measured once daily. Five days following virus challenge, all animals were humanely euthanized, and the nasal turbinate and lung tissue were collected. Tissues were homogenized in sterile PBS using a handheld tissue homogenizer (Omni International) and stored at −80°C for virus titration.

SARS-CoV-2 virus titration from mouse tissues by $TCID_{50}$ assay

Vero E6 cells (ATCC no. CRL-1586) were seeded at a density of 20,000 cells per well into 96-well flat-bottomed tissue culture plates (Nunc) and incubated overnight at 37°C with 5% CO_2 and humidity. Homogenized tissues were centrifuged at 8000 rpm for 10 min at 4°C, and the supernatant was collected and serially diluted 10-fold (up to 10^{-7}) in viral growth medium (DMEM containing 5% FBS and 1% antibiotic/antimycotic solution). After overnight incubation, the cell plates were washed twice with PBS, and the serial dilutions were added to each well in quadruplicate. The plates were further incubated at 37°C in a humidified incubator with 5% CO_2. After 3 days, cells were stained with 0.1% crystal violet containing 10% neutral-buffered formalin and scored for cytopathic effect development. The median tissure culture infectious dose ($TCID_{50}$) was calculated as per Reed and Muench method (*44*) and corrected for per-gram weight of each lung homogenate. All animal work was approved by the University of Louisville Institutional Animal Care and Use Committee. All work with live SARS-CoV-2 was approved by the University Institutional Biosafety Committee and conducted within biosafety level 3 containment.

Analysis of patient data

All patient data analysis was approved by the N3C and the University of Chicago Biological Sciences Division IRB (IRB21-0591), which granted a waiver of consent because the identities of the study participants cannot readily be ascertained by the investigators, the investigators do not contact the participants, and the investigators will not reidentify participants. A detailed description of the patient data analysis methods and findings is in the Patient Data Analysis Supplement.

Statistical analysis

Data are shown as means ± SD. For RNA-seq differential expression analysis, DESeq2 version 1.22.1 was used with a minimum false discovery rate–corrected *P* value (*q* value) significance threshold of 0.01 for the RNA-seq experiment involving CBD and SARS-CoV-2 and a threshold of 0.05 for the RNA-seq experiment involving CBDV and SARS-CoV-2. For GSEA, Metascape was used with a minimum *P*-value significance threshold of 0.05. For EC_{50} calculations of drug treatments, GraphPad Prism software was used with a nonlinear curve fit with four parameters. Prism was also used for unpaired *t* tests, and one-way ANOVA with statistical significance was defined as $P < 0.05$. For the patient data statistical analysis methods, please refer to the "Statistical analysis" section of the Patient Data Analysis Supplement.

SUPPLEMENTARY MATERIALS

Supplementary material for this article is available at https://science.org/doi/10.1126/sciadv.abi6110

View/request a protocol for this paper from *Bio-protocol*.

REFERENCES AND NOTES

1. S. R. Weiss, J. L. Leibowitz, Coronavirus pathogenesis. *Adv. Virus Res.* **81**, 85–164 (2011).
2. S. E. Galloway, P. Paul, D. R. MacCannell, M. A. Johansson, J. T. Brooks, A. M. Neil, R. B. Slayton, S. Tong, B. J. Silk, G. L. Armstrong, M. Biggerstaff, V. G. Dugan, Emergence

of SARS-CoV-2 B.1.1.7 lineage - United States, December 29, 2020-January 12, 2021. *MMWR Morb. Mortal. Wkly Rep.* **70**, 95–99 (2021).
3. M. Hoffmann, H. Kleine-Weber, S. Schroeder, N. Krüger, T. Herrler, S. Erichsen, T. S. Schiergens, G. Herrler, N.-H. Wu, A. Nitsche, M. A. Müller, C. Drosten, S. Pöhlmann, SARS-CoV-2 cell entry depends on ACE2 and TMPRSS2 and is blocked by a clinically proven protease inhibitor. *Cell* **181**, 271–280.e8 (2020).
4. J. Jaimes, J. Millet, G. Whittaker, Proteolytic cleavage of the SARS-CoV-2 spike protein and the role of the novel S1/S2 Site. *iScience* **23**, 101212 (2020).
5. S. Matsuyama, N. Nao, K. Shirato, M. Kawase, S. Saito, I. Takayama, N. Nagata, T. Sekizuka, H. Katoh, F. Kato, M. Sakata, M. Tahara, S. Kutsuna, N. Ohmagari, M. Kuroda, T. Suzuki, T. Kageyama, M. Takeda, Enhanced isolation of SARS-CoV-2 by TMPRSS2-expressing cells. *Proc. Natl. Acad. Sci. U.S.A.* **117**, 7001–7003 (2020).
6. R. Wang, C. R. Simoneau, J. Kulsuptrakul, M. Bouhaddou, K. A. Travisano, J. M. Hayashi, J. Carlson-Stevermer, J. R. Zengel, C. M. Richards, P. Fozouni, J. Oki, L. Rodriguez, B. Joehnk, K. Walcott, K. Holden, A. Sil, J. E. Carette, N. J. Krogan, M. Ott, Genetic screens identify host factors for SARS-CoV-2 and common cold coronaviruses. *Cell* **184**, 106–119.e14 (2021).
7. W. M. Schneider, J. M. Luna, H.-H. Hoffmann, F. J. Sánchez-Rivera, A. A. Leal, A. W. Ashbrook, J. L. Pen, I. Ricardo-Lax, E. Michailidis, A. Peace, A. F. Stenzel, S. W. Lowe, M. R. MacDonald, C. M. Rice, J. T. Poirier, Genome-scale identification of SARS-CoV-2 and pan-coronavirus host factor networks. *Cell* **184**, 120–132.e14 (2021).
8. Z. Daniloski, T. X. Jordan, H.-H. Wessels, D. A. Hoagland, S. Kasela, M. Legut, S. Maniatis, E. P. Mimitou, L. Lu, E. Geller, O. Danziger, B. R. Rosenberg, H. Phatnani, P. Smibert, T. Lappalainen, B. R. tenOever, N. E. Sanjana, Identification of required host factors for SARS-CoV-2 infection in human cells. *Cell* **184**, 92–105.e16 (2021).
9. D. W. Kneller, G. Phillips, H. M. O'Neill, R. Jedrzejczak, L. Stols, P. Langan, A. Joachimiak, L. Coates, A. Kovalevsky, Structural plasticity of SARS-CoV-2 3CL Mpro active site cavity revealed by room temperature x-ray crystallography. *Nat. Commun.* **11**, 3202 (2020).
10. J. Osipiuk, S. A. Azizi, S. Dvorkin, M. Endres, R. Jedrzejczak, K. A. Jones, S. Kang, R. S. Kathayat, Y. Kim, V. G. Lisnyak, S. L. Maki, V. Nicolaescu, C. A. Taylor, C. Tesar, Y. A. Zhang, Z. Zhou, G. Randall, K. Michalska, S. A. Snyder, B. C. Dickinson, A. Joachimiak, Structure of papain-like protease from SARS-CoV-2 and its complexes with non-covalent inhibitors. *Nat. Commun.* **12**, 743 (2021).
11. F. Shahbazi, V. Grandi, A. Banerjee, J. F. Trant, Cannabinoids and cannabinoid receptors: The story so far. *iScience* **23**, 101301 (2020).
12. K. M. Nelson, J. Bisson, G. Singh, J. G. Graham, S. N. Chen, J. B. Friesen, J. L. Dahlin, M. Niemitz, M. A. Walters, G. F. Pauli, The essential medicinal chemistry of cannabidiol (CBD). *J. Med. Chem.* **63**, 12137–12155 (2020).
13. K. Sekar, A. Pack, Epidiolex as adjunct therapy for treatment of refractory epilepsy: A comprehensive review with a focus on adverse effects. *F1000Res* **8**, F1000 (2019).
14. H. I. Lowe, N. J. Toyang, W. McLaughlin, Potential of cannabidiol for the treatment of viral hepatitis. *Pharm. Res.* **9**, 116–118 (2017).
15. L. Taylor, B. Gidal, G. Blakey, B. Tayo, G. Morrison, A phase I, randomized, double-blind, placebo-controlled, single ascending dose, multiple dose, and food effect trial of the safety, tolerability and pharmacokinetics of highly purified cannabidiol in healthy subjects. *CNS Drugs* **32**, 1053–1067 (2018).
16. S. M. Anil, N. Shalev, A. C. Vinayaka, S. Nadarajan, D. Namdar, E. Belausov, I. Shoval, K. A. Mani, G. Mechrez, H. Koltai, *Cannabis* compounds exhibit anti-inflammatory activity in vitro in COVID-19-related inflammation in lung epithelial cells and pro-inflammatory activity in macrophages. *Sci. Rep.* **11**, 1462 (2021).
17. K. H. D. Crawford, R. Eguia, A. S. Dingens, A. N. Loes, K. D. Malone, C. R. Wolf, H. Y. Chu, M. A. Tortorici, D. Veesler, M. Murphy, D. Pettie, N. P. King, A. B. Balazs, J. D. Bloom, Protocol and reagents for pseudotyping lentiviral particles with SARS-CoV-2 spike protein for neutralization assays. *Viruses* **12**, 513 (2020).
18. C. Hetz, E. Chevet, S. A. Oakes, Proteostasis control by the unfolded protein response. *Nat. Cell Biol.* **17**, 829–838 (2015).
19. R. Dash, M. C. Ali, I. Jahan, Y. A. Munni, S. Mitra, M. A. Hannan, B. Timalsina, D. F. Oktaviani, H. J. Choi, I. S. Moon, Emerging potential of cannabidiol in reversing proteinopathies. *Ageing Res. Rev.* **65**, 101209 (2021).
20. J. Bechill, Z. Chen, J. W. Brewer, S. C. Baker, Mouse hepatitis virus infection activates the Ire1/XBP1 pathway of the unfolded protein response. *Adv. Exp. Med. Biol.* **581**, 139–144 (2006).
21. T. S. Fung, D. X. Liu, The ER stress sensor IRE1 and MAP kinase ERK modulate autophagy induction in cells infected with coronavirus infectious bronchitis virus. *Virology* **533**, 34–44 (2019).
22. C. Hetz, K. Zhang, R. J. Kaufman, Mechanisms, regulation and functions of the unfolded protein response. *Nat. Rev. Mol. Cell Biol.* **21**, 421–438 (2020).
23. O. Haller, G. Kochs, F. Weber, The interferon response circuit: Induction and suppression by pathogenic viruses. *Virology* **344**, 119–130 (2006).
24. D. Blanco-Melo, B. E. Nilsson-Payant, W.-C. Liu, S. Uhl, D. Hoagland, R. Møller, T. X. Jordan, K. Oishi, M. Panis, D. Sachs, T. T. Wang, R. E. Schwartz, J. K. Lim, R. A. Albrecht, B. R. tenOever, Imbalanced host response to SARS-CoV-2 drives development of COVID-19. *Cell* **181**, 1036–1045.e9 (2020).
25. H. Di, H. Elbahesh, M. A. Brinton, Characteristics of human OAS1 isoform proteins. *Viruses* **12**, (2020).
26. T. A. Tummino, V. V. Rezelj, B. Fischer, A. Fischer, M. J. O'Meara, B. Monel, T. Vallet, Z. Zhang, A. Alon, H. R. O'Donnell, J. Lyu, H. Schadt, K. M. White, N. J. Krogan, L. Urban, K. M. Shokat, A. C. Kruse, A. García-Sastre, O. Schwartz, F. Moretti, M. Vignuzzi, F. Pognan, B. K. Shoichet, Phospholipidosis is a shared mechanism underlying the in vitro antiviral activity of many repurposed drugs against SARS-CoV-2. *bioRxiv* 10.1101/2021.03.23.436648 , (2021).
27. P. B. McCray Jr., L. Pewe, C. Wohlford-Lenane, M. Hickey, L. Manzel, L. Shi, J. Netland, H. P. Jia, C. Halabi, C. D. Sigmund, D. K. Meyerholz, P. Kirby, D. C. Look, S. Perlman, Lethal infection of K18-hACE2 mice infected with severe acute respiratory syndrome coronavirus. *J. Virol.* **81**, 813–821 (2007).
28. M. A. Haendel, C. G. Chute, T. D. Bennett, D. A. Eichmann, J. Guinney, W. A. Kibbe, P. R. O. Payne, E. R. Pfaff, P. N. Robinson, J. H. Saltz, H. Spratt, C. Suver, J. Wilbanks, A. B. Wilcox, A. E. Williams, C. Wu, C. Blacketer, R. L. Bradford, J. J. Cimino, M. Clark, E. W. Colmenares, P. A. Francis, D. Gabriel, A. Graves, R. Hemadri, S. S. Hong, G. Hripscak, D. Jiao, J. G. Klann, K. Kostka, A. M. Lee, H. P. Lehmann, L. Lingrey, R. T. Miller, M. Morris, S. N. Murphy, K. Natarajan, M. B. Palchuk, U. Sheikh, H. Solbrig, S. Visweswaran, A. Walden, K. M. Walters, G. M. Weber, X. T. Zhang, R. L. Zhu, B. Amor, A. T. Girvin, A. Manna, N. Qureshi, M. G. Kurilla, S. G. Michael, L. M. Portilla, J. L. Rutter, C. P. Austin, K. R. Gersing; The N3C Consortium, The National COVID Cohort Collaborative (N3C): Rationale, design, infrastructure, and deployment. *J. Am. Med. Inform. Assoc.* **28**, 427–443 (2021).
29. Centers for Disease Control and Prevention, *COVID-19, People at Increased Risk, People with Certain Medical Conditions* (CDC, 2021).
30. Q. Zhou, V. Chen, C. P. Shannon, X. S. Wei, X. Xiang, X. Wang, Z. H. Wang, S. J. Tebbutt, T. R. Kollmann, E. N. Fish, Interferon-α2b teatment for COVID-19. *Front. Immunol.* **11**, 1061 (2020).
31. T. Muthumalage, I. Rahman, Cannabidiol differentially regulates basal and LPS-induced inflammatory responses in macrophages, lung epithelial cells, and fibroblasts. *Toxicol. Appl. Pharmacol.* **382**, 114713 (2019).
32. Food and Drug Administration (FDA), Application number 210365Orig1s000, *Clinical Pharmacology and Biopharmaceutics Reviews* (2017).
33. B. C. Sorkin, A. J. Kuszak, G. Bloss, N. K. Fukagawa, F. A. Hoffman, M. Jafari, B. Barrett, P. N. Brown, F. D. Bushman, S. J. Casper, F. H. Chilton, C. S. Coffey, M. G. Ferruzzi, D. C. Hopp, M. Kiely, D. Lakens, J. B. MacMillan, D. O. Meltzer, M. Pahor, J. Paul, K. Pritchett-Corning, S. K. Quinney, B. Rehermann, K. D. R. Setchell, N. S. Sipes, J. M. Stephens, D. L. Taylor, H. Tiriac, M. A. Walters, D. Xi, G. Zappalá, G. F. Pauli, Improving natural product research translation: From source to clinical trial. *FASEB J.* **34**, 41–65 (2020).
34. E. Afgan, D. Baker, B. Batut, M. van den Beek, D. Bouvier, M. Čech, J. Chilton, D. Clements, N. Coraor, B. A. Grüning, A. Guerler, J. Hillman-Jackson, S. Hiltemann, V. Jalili, H. Rasche, N. Soranzo, J. Goecks, J. Taylor, A. Nekrutenko, D. Blankenberg, The Galaxy platform for accessible, reproducible and collaborative biomedical analyses: 2018 update. *Nucleic Acids Res.* **46**, W537–W544 (2018).
35. F. Krueger, Trim Galore, A wrapper tool around Cutadapt and FastQC to consistently apply quality and adapter trimming to FastQ files. (2015); https://www.bioinformatics.babraham.ac.uk/projects/trim_galore/.
36. A. Dobin, C. A. Davis, F. Schlesinger, J. Drenkow, C. Zaleski, S. Jha, P. Batut, M. Chaisson, T. R. Gingeras, STAR: Ultrafast universal RNA-seq aligner. *Bioinformatics* **29**, 15–21 (2013).
37. Y. Liao, G. K. Smyth, W. Shi, featureCounts: An efficient general purpose program for assigning sequence reads to genomic features. *Bioinformatics* **30**, 923–930 (2014).
38. M. I. Love, W. Huber, S. Anders, Moderated estimation of fold change and dispersion for RNA-seq data with DESeq2. *Genome Biol.* **15**, 550 (2014).
39. J. T. Robinson, H. Thorvaldsdóttir, W. Winckler, M. Guttman, E. S. Lander, G. Getz, J. P. Mesirov, Integrative genomics viewer. *Nat. Biotechnol.* **29**, 24–26 (2011).
40. S. B. Yoon, Y. H. Park, S. A. Choi, H. J. Yang, P. S. Jeong, J. J. Cha, S. Lee, S. H. Lee, J. H. Lee, B. W. Sim, B. S. Koo, S. J. Park, Y. Lee, Y. H. Kim, J. J. Hong, J. S. Kim, Y. B. Jin, J. W. Huh, S. R. Lee, B. S. Song, S. U. Kim, Real-time PCR quantification of spliced X-box binding protein 1 (XBP1) using a universal primer method. *PLOS ONE* **14**, e0219978 (2019).
41. Y. Zhou, B. Zhou, L. Pache, M. Chang, A. H. Khodabakhshi, O. Tanaseichuk, C. Benner, S. K. Chanda, Metascape provides a biologist-oriented resource for the analysis of systems-level datasets. *Nat. Commun.* **10**, 1523 (2019).
42. A. Subramanian, P. Tamayo, V. K. Mootha, S. Mukherjee, B. L. Ebert, M. A. Gillette, A. Paulovich, S. L. Pomeroy, T. R. Golub, E. S. Lander, J. P. Mesirov, Gene set enrichment analysis: A knowledge-based approach for interpreting genome-wide expression profiles. *Proc. Natl. Acad. Sci. U.S.A.* **102**, 15545–15550 (2005).
43. C. Hetz, F. Martinon, D. Rodriguez, L. H. Glimcher, The unfolded protein response: Integrating stress signals through the stress sensor IRE1α. *Physiol. Rev.* **91**, 1219–1243 (2011).

44. L. J. Reed, H. Muench, A simple method of estimating 50% end points. *Am. J. Epidemiol.* **27**, 493–497 (1938).
45. Observational Health Data Sciences and Informatics, ATLAS (2021); www.ohdsi.org/software-tools/atlas/.
46. Observational Medical Outcomes Partnership (OMOP), OMOP Clinical Data Model v5.3.1, Standardized Derived Elements, Drug Era table (2021); https://ohdsi.github.io/CommonDataModel/cdm53.html#Standardized_Derived_Elements.
47. Centers for Disease Control and Prevention, *COVID-19: When to Quarantine* (CDC, 2021).
48. Text Processing Services Library, *Regular Expression Operations* (Python Software Foundation, 2021); https://docs.python.org/3/library/re.html.
49. J. J. Beltran-Montoya, T. Herrerias-Canedo, A. Arzola-Paniagua, F. Vadillo-Ortega, O. F. Dueñas-Garcia, H. Rico-Olvera, A randomized, clinical trial of ketorolac tromethamine vs ketorolac trometamine plus complex B vitamins for cesarean delivery analgesia. *Saudi J Anaesth* **6**, 207–212 (2012).
50. Centers for Disease Control and Prevention, *COVID-19-Hospitalization and Death by Age* (CDC, 2021).
51. Observational Medical Outcomes Partnership (OMOP), OMOP Clinical Data Model v5.3.1, Clinical Data Tables, Person table (2021); https://ohdsi.github.io/CommonDataModel/cdm53.html.
52. L. Kompaniyets, A. B. Goodman, B. Belay, D. S. Freedman, M. S. Sucosky, S. J. Lange, A. V. Gundlapalli, T. K. Boehmer, H. M. Blanck, Body mass index and risk for COVID-19–related hospitalization, intensive care unit admission, invasive mechanical ventilation, and Death—United States, March–December 2020. *MMWR Morb. Mortal. Wkly Rep.* **70**, 355–361 (2021).
53. C. B. Weir, A. Jan, BMI classification percentile and cut off points. In: *StatPearls* [*Internet*] (StatPearls Publishing, January 2021, updated 9 May 2021); https://www.ncbi.nlm.nih.gov/books/NBK541070/.
54. US Food and Drug Administration, FDA approves new indication for drug containing an active ingredient derived from cannabis to treat seizures in rare genetic Disease (FDA news release, 31 July 2020); https://www.fda.gov/news-events/press-announcements/fda-approves-new-indication-drug-containing-active-ingredient-derived-cannabis-treat-seizures-rare.
55. E. C. Leas, E. M. Hendrickson, A. L. Nobles, R. Todd, D. M. Smith, M. Dredze, J. W. Ayers, Self-reported cannabidiol (CBD) use for conditions with proven therapies. *JAMA Netw. Open* **3**, e2020977 (2020).
56. M. Hepburn, N. Mullaguri, P. George, S. Hantus, V. Punia, A. Bhimraj, C. R. Newey, Acute symptomatic seizures in critically ill patients with COVID-19: Is there an association? *Neurocrit. Care* **34**, 139–143 (2021).
57. StataCorp, Tabulate two-way reference manual (2021); https://www.stata.com/manuals/rtabulatetwoway.pdf.
58. D. Ho, K. Imai, G. King, E. A. Stuart, MatchIt: nonparametric preprocessing for parametric causal inference. *J. Stat. Softw.* **42**, 1–28 (2021).
59. P. C. Austin, Balance diagnostics for comparing the distribution of baseline covariates between treatment groups in propensity-score matched samples. *Stat. Med.* **28**, 3083–3107 (2009).
60. D. Pregibon, Data Analytic Methods for Generalized Linear Models. Thesis, University of Toronto (1979).
61. L. Blizzard, D. W. Hosmer, Parameter estimation and goodness-of-fit in log binomial regression. *Biom. J.* **48**, 5–22 (2006).
62. John Hopkins Coronavirus Resource Center, Covid-19 Dashboard. (2021); https://coronavirus.jhu.edu/map.html.
63. National COVID Cohort Collaborative, *COVID-19 Phenotype 3.0 Additional Information* (N3C, 2021); https://github.com/National-COVID-Cohort-Collaborative/Phenotype_Data_Acquisition/wiki/Phenotype-3.0.

Acknowledgments: *Overall*. The following reagent was deposited by the CDC and obtained through BEI Resources, NIAID, NIH: SARS-related coronavirus 2, isolate USA-WA1/2020, NR-52281. Figure 8A was created using BioRender.com. We thank the members of the SARS-CoV-2 host response team in Chicago for stimulating discussions and support with particular thanks to J. Solway, R. Morimoto, N. Hay, A. Sperling, H.H. Chen, R. Lee, R. Roos, S. Elf, A. Muir, G. Mutlu, J. Pinto, S. White, N. Dulin, R. Moellering, V. Natarajan, L. Platanias, and K. Ridge. We thank D. Missiakas for facilitating access to the University of Chicago Howard Taylor Ricketts Facility by providing protocols and trained scientists. We also thank N. Rosner and K. Cagney for proposing and facilitating analysis of clinical data, M. Ratain for consideration of pharmacokinetic issues, and K. Igarashi for discussions. We thank the University of Chicago Genomics Facility (RRID:SCR_019196) especially S. Arun and P. Faber for assistance with RNA-seq. Last, we would like to acknowledge the University of Chicago Vice Provost for Research, K. Kim, and the Dean of the Biological Sciences Division, K. Polonsky, for steadfast support.

National COVID Cohort Collaborative (N3C). The patient data analyses described in this publication were conducted with data or tools accessed through the NCATS N3C Data Enclave covid.cd2h.org/enclave and supported by NCATS U24 TR002306. This research was possible because of the patients whose information is included within the data from participating organizations (covid.cd2h.org/dtas) and the organizations (https://ncats.nih.gov/n3c/resources/data-contribution/data-transfer-agreement-signatories) and scientists who have contributed to the on-going development of this community resource (*28*). The project described was supported by the National Institute of General Medical Sciences, 5U54GM104942-04. The content is solely the responsibility of the authors and does not necessarily represent the official views of the NIH. The analysis used only deidentified data (i.e., N3C Data Access Tier 2, described at https://covid.cd2h.org/N3C_governance). We gratefully acknowledge contributions from the following N3C core teams:

• *Principal investigators*: M. A. Haendel, C. G. Chute, K. R. Gersing, and A. Walden.
• *Workstream, subgroup, and administrative leaders*: M. A. Haendel, T. D. Bennett, C. G. Chute, D. A. Eichmann, J. Guinney, W. A. Kibbe, H. Liu, P. R.O. Payne, E. R. Pfaff, P. N. Robinson, J. H. Saltz, H. Spratt, J. Starren, C. Suver, A. B. Wilcox, A. E. Williams, and C. Wu.
• *Key liaisons at data partner sites*
• *Regulatory staff at data partner sites*
• *Individuals at the sites who are responsible for creating the datasets and submitting data to N3C*
• *Data ingest and harmonization team*: C. G. Chute, E. R. Pfaff, D. Gabriel, S. S. Hong, K. Kostka, H. P. Lehmann, R. A. Moffitt, M. Morris, M. B. Palchuk, X. T. Zhang, and R. L. Zhu.
• *Phenotype team (individuals who create the scripts that the sites use to submit their data, based on the COVID and long COVID definitions)*: E. R. Pfaff, B. Amor, M. M. Bissell, M. Clark, A. T. G., S. S. Hong, K. Kostka, A. M. Lee, R. T. Miller, M. Morris, M. B. Palchuk, and K. M. Walters.
• *Project management and operations team*: A. Walden, Y. Chae, C. Cook, A. Dest, R. R. Dietz, T. Dillon, P. A. Francis, R. Fuentes, A. Graves, J. A. McMurry, A. J. Neumann, S. T. O'Neil, U. Sheikh, A. M. Volz, and E. Zampino.
• *Partners from NIH and other federal agencies*: C. P. Austin, K. R. Gersing, S. Bozzette, M. Deacy, N. Garbarini, M. G. Kurilla, S. G. Michael, J. L. Rutter, and M. Temple-O'Connor.
• *Analytics team (individuals who build the Enclave infrastructure, help create codesets and variables, and help domain teams and project teams with their datasets)*: B. Amor, M. M. Bissell, K. R. Bradwell, A. T. Girvin, A. Manna, and N. Qureshi.
• *Publication committee management team*: M. M. Saltz, C. Suver, C. G. Chute, M. A. Haendel, J. A. McMurry, A. M. Volz, and A. Walden
• *Publication committee review team*: C. Bramante, J. R. Harper, W. Hernandez, F. M. Koraishy, F. Mariona, S. Mattapally, A. Saha, and S. Vedula
• *Data partners with released data (50)*: Stony Brook University—U24TR002306 • University of Oklahoma Health Sciences Center—U54GM104938: Oklahoma Clinical and Translational Science Institute (OCTSI) • West Virginia University—U54GM104942: West Virginia Clinical and Translational Science Institute (WVCTSI) • University of Mississippi Medical Center—U54GM115428: Mississippi Center for Clinical and Translational Research (CCTR) • University of Nebraska Medical Center—U54GM115458: Great Plains IDeA-Clinical and Translational Research • Maine Medical Center—U54GM115516: Northern New England Clinical and Translational Research (NNE-CTR) Network • Wake Forest University Health Sciences—UL1TR001420: Wake Forest Clinical and Translational Science Institute • Northwestern University at Chicago—UL1TR001422: Northwestern University Clinical and Translational Science Institute (NUCATS) • University of Cincinnati—UL1TR001425: Center for Clinical and Translational Science and Training • The University of Texas Medical Branch at Galveston—UL1TR001439: The Institute for Translational Sciences • Medical University of South Carolina—UL1TR001450: South Carolina Clinical and Translational Research Institute (SCTR) • University of Massachusetts Medical School Worcester—UL1TR001453: The UMass Center for Clinical and Translational Science (UMCCTS) • University of Southern California—UL1TR001855: The Southern California Clinical and Translational Science Institute (SC CTSI) • Columbia University Irving Medical Center—UL1TR001873: Irving Institute for Clinical and Translational Research • George Washington Children's Research Institute—UL1TR001876: Clinical and Translational Science Institute at Children's National (CTSA-CN) • University of Kentucky—UL1TR001998: UK Center for Clinical and Translational Science • University of Rochester—UL1TR002001: UR Clinical and Translational Science Institute • University of Illinois at Chicago—UL1TR002003: UIC Center for Clinical and Translational Science • Penn State Health Milton S. Hershey Medical Center—UL1TR002014: Penn State Clinical and Translational Science Institute • The University of Michigan at Ann Arbor—UL1TR002240: Michigan Institute for Clinical and Health Research • Vanderbilt University Medical Center—UL1TR002243: Vanderbilt Institute for Clinical and Translational Research • University of Washington—UL1TR002319: Institute of Translational Health Sciences • Washington University in St. Louis—UL1TR002345: Institute of Clinical and Translational Sciences • Oregon Health and Science University—UL1TR002369: Oregon Clinical and Translational Research Institute • University of Wisconsin-Madison—UL1TR002373: UW Institute for Clinical and Translational Research • Rush University Medical Center—UL1TR002389: The Institute for Translational Medicine (ITM) • The University of Chicago—UL1TR002389:

The Institute for Translational Medicine (ITM) • University of North Carolina at Chapel Hill—UL1TR002489: North Carolina Translational and Clinical Science Institute • University of Minnesota—UL1TR002494: Clinical and Translational Science Institute • Children's Hospital Colorado—UL1TR002535: Colorado Clinical and Translational Sciences Institute • The University of Iowa—UL1TR002537: Institute for Clinical and Translational Science • The University of Utah—UL1TR002538: Uhealth Center for Clinical and Translational Science • Tufts Medical Center—UL1TR002544: Tufts Clinical and Translational Science Institute • Duke University—UL1TR002553: Duke Clinical and Translational Science Institute • Virginia Commonwealth University—UL1TR002649: C. Kenneth and Dianne Wright Center for Clinical and Translational Research • The Ohio State University—UL1TR002733: Center for Clinical and Translational Science • The University of Miami Leonard M. Miller School of Medicine—UL1TR002736: University of Miami Clinical and Translational Science Institute • University of Virginia—UL1TR003015: iTHRIVL Integrated Translational health Research Institute of Virginia • Carilion Clinic—UL1TR003015: iTHRIVL Integrated Translational health Research Institute of Virginia • University of Alabama at Birmingham—UL1TR003096: Center for Clinical and Translational Science • Johns Hopkins University—UL1TR003098: Johns Hopkins Institute for Clinical and Translational Research • University of Arkansas for Medical Sciences—UL1TR003107: UAMS Translational Research Institute • Nemours—U54GM104941: Delaware CTR ACCEL Program • University Medical Center New Orleans—U54GM104940: Louisiana Clinical and Translational Science (LA CaTS) Center • University of Colorado Denver, Anschutz Medical Campus—UL1TR002535: Colorado Clinical and Translational Sciences Institute • Mayo Clinic Rochester—UL1TR002377: Mayo Clinic Center for Clinical and Translational Science (CCaTS) • Tulane University—UL1TR003096: Center for Clinical and Translational Science • Loyola University Medical Center—UL1TR002389: The Institute for Translational Medicine (ITM) • Advocate Health Care Network—UL1TR002389: The Institute for Translational Medicine (ITM) • OCHIN—INV-018455: Bill and Melinda Gates Foundation grant to Sage Bionetworks • *Additional data partners who have signed DTA and data release pending* (*35*)**:** The Rockefeller University—UL1TR001866: Center for Clinical and Translational Science • The Scripps Research Institute—UL1TR002550: Scripps Research Translational Institute • University of Texas Health Science Center at San Antonio—UL1TR002645: Institute for Integration of Medicine and Science • The University of Texas Health Science Center at Houston—UL1TR003167: Center for Clinical and Translational Sciences (CCTS) • NorthShore University HealthSystem—UL1TR002389: The Institute for Translational Medicine (ITM) • Yale New Haven Hospital—UL1TR001863: Yale Center for Clinical Investigation • Emory University—UL1TR002378: Georgia Clinical and Translational Science Alliance • Weill Medical College of Cornell University—UL1TR002384: Weill Cornell Medicine Clinical and Translational Science Center • Montefiore Medical Center—UL1TR002556: Institute for Clinical and Translational Research at Einstein and Montefiore • Medical College of Wisconsin—UL1TR001436: Clinical and Translational Science Institute of Southeast Wisconsin • University of New Mexico Health Sciences Center—UL1TR001449: University of New Mexico Clinical and Translational Science Center • George Washington University—UL1TR001876: Clinical and Translational Science Institute at Children's National (CTSA-CN) • Stanford University—UL1TR003142: Spectrum: The Stanford Center for Clinical and Translational Research and Education • Regenstrief Institute—UL1TR002529: Indiana Clinical and Translational Science Institute • Cincinnati Children's Hospital Medical Center—UL1TR001425: Center for Clinical and Translational Science and Training • Boston University Medical Campus—UL1TR001430: Boston University Clinical and Translational Science Institute • The State University of New York at Buffalo—UL1TR001412: Clinical and Translational Science Institute • Aurora Health Care—UL1TR002373: Wisconsin Network For Health Research • Brown University—U54GM115677: Advance Clinical Translational Research (Advance-CTR) • Rutgers, The State University of New Jersey—UL1TR003017: New Jersey Alliance for Clinical and Translational Science • Loyola University Chicago—UL1TR002389: The Institute for Translational Medicine (ITM) • New York University—UL1TR001445: Langone Health's Clinical and Translational Science Institute • Children's Hospital of Philadelphia—UL1TR001878: Institute for Translational Medicine and Therapeutics • University of Kansas Medical Center—UL1TR002366: Frontiers: University of Kansas Clinical and Translational Science Institute • Massachusetts General Brigham—UL1TR002541: Harvard Catalyst • Icahn School of Medicine at Mount Sinai—UL1TR001433: ConduITS Institute for Translational Sciences • Ochsner Medical Center—U54GM104940: Louisiana Clinical and Translational Science (LA CaTS) Center • HonorHealth—None (Voluntary) • University of California, Irvine—UL1TR001414: The UC Irvine Institute for Clinical and Translational Science (ICTS) • University of California, San Diego—UL1TR001442: Altman Clinical and Translational Research Institute • University of California, Davis—UL1TR001860: UCDavis Health Clinical and Translational Science Center • University of California, San Francisco—UL1TR001872: UCSF Clinical and Translational Science Institute • University of California, Los Angeles—UL1TR001881: UCLA Clinical Translational Science Institute • University of Vermont—U54GM115516: Northern New England Clinical & Translational Research (NNE-CTR) Network • Arkansas Children's Hospital—UL1TR003107: UAMS Translational Research Institute

• *Additional N3C acknowledgments***:** We would also like to thank others not listed above: J. Alamgir (ARIScience), S. Russell (University of Colorado), and H. Zhang, (University of Chicago), who created N3C concept sets that we used to define some of the medical condition indicator covariates for our statistical analysis. We would also like to thank S. Johnson (University of Minnesota) for writing a BMI calculation Knowledge Object that we modified for calculating BMI values from weight and height data.

Funding: This work was supported directly by BIG Vision grant from the University of Chicago (to M.R.R.); NIH grants R01 GM121735 (to M.R.R.), R01 CA184494 (to M.R.R.), R01 AI137514 (to G.R.), R01 AI127518 (to G.R.), R01 AI134980 (to G.R.), R01 CA219815 (to S.A.O.), R35 GM119840 (to B.C.D), and P30 CA014599 (University of Chicago Comprehensive Cancer Center Support grant); and Harry B. and Leona M. Helmsley Charitable Trust (to K.E.P). The NMR analysis component of this work was supported indirectly by Jeol Resonance, Peabody, MA (G.F.P.). The patient analysis component of this work was supported indirectly by the funding listed in the N3C section of the Acknowledgments section. **Author contributions:** Conceptualization: M.R.R., L.C.N., D.Y., G.R., S.A.O., G.F.P., D.O.M., N.D., and T.J.B. Methodology: M.R.R., L.C.N., D.Y., G.R., S.A.O., D.O.M., G.F.P., N.D., B.C.D., and T.J.B. Software: D.Y. and T.J.B. Formal analysis: D.Y. and T.J.B. Investigation: L.C.N., D.Y., V.N., T.J.B., T.O., S.-N.C., J.B.F., and N.D., A.M., C.D., D.Si., H.G., L.S., L.R.-M., A.V., E.S., K.A.J., and S.-A.A. Resources: G.R., M.R.R., G.F.P., S.T., and B.C.D. Data curation: D.O.M., T.J.B., D.Y., and the N3C Consortium. Writing—original draft: M.R.R. Writing—review and editing: L.C.N., D.Y., V.N., T.J.B., S.-N.C., J.B.F., N.D., A.M., K.A.J., D.Si., J.M.M., B.C.D., S.T., S.A.O., G.F.P., D.O.M., G.R., and M.R.R. Visualization: L.C.N., D.Y., N.D., A.M., S.-N.C., B.C.D., and J.B.F. Supervision: M.R.R., G.R., D.O.M., G.F.P., S.A.O., S.T., and B.C.D. Project administration: M.R.R. Funding acquisition: M.R.R. For the animal experiment: Investigation: D.Sa. and C.D.A. Formal analysis: D.Sa. and J.D.G. Methodology: J.D.G., J.K.D., D.Sa., W.E.S., and K.E.P. Obtaining approvals: W.E.S. and J.D.G. Funding acquisition: K.E.P. **Competing interests:** S.A.O. is a cofounder and consultant at OptiKira. L.L.C. (Cleveland, OH). The authors declare that they have no other competing interests. **Data and materials availability:** All data needed to evaluate the conclusions in the paper are present in the paper and/or the Supplementary Materials. Raw and processed RNA-seq data were deposited into the GEO database (GSE168797).

Submitted 19 March 2021
Accepted 29 December 2021
Published First Relase 20 January 2022
Published 23 February 2022
10.1126/sciadv.abi6110